Seismic Analysis and Petrophysical Evaluation of the Pennsylvanian Rasberry Reef Phylloid Algal Carbonate Mounds in the Knox-Baylor Trough, Knox County, Texas

by

WILLIAM HOFFMAN

Presented to the Faculty of the Graduate School of
The University of Texas at Arlington In Partial Fulfillment
of the Requirements
for the Degree of

MASTER OF SCIENCE IN PETROLEUM GEOSCIENCE

The University of Texas at Arlington
May 2018

Acknowledgements

I would first like to thank Steve Miller and Eddie Loudon for providing me with the data for my thesis. Without this data, I would not have gained the experience I wished to attain with Kingdom and Petra. I would further like to thank Eddie for the guidance and advice he provided throughout the project. I would like to thank my advisor, Bill Moulton. I am grateful for the constant help and knowledge he provided. I would also like to thank my other committee members, Dr. Qinhong Hu and Dr. John Wickham. Finally, I would like to thank my parents for their constant support. I would not have made it this far in my education without them.

January 15, 2018

Abstract

Seismic Analysis and Petrophysical Evaluation of the Pennsylvanian Rasberry Reef Phylloid Algal Carbonate Mounds in the Knox-Baylor Trough, Knox County, Texas

William Hoffman, MS

The University of Texas at Arlington, 2018

Supervising Professor: Qinhong Hu

The Ellis Ranch Wildcat field in Knox County, Texas produces from an isolated carbonate platform located on the northern flank of the Knox-Baylor Trough. The platform is composed of the Desmoinesian aged Caddo Limestone and Rasberry Reef. The Rasberry Reef contains aragonitic, phylloid algal bafflestone mounds that form excellent hydrocarbon reservoirs. Aragonitic grains are prone to dissolution during burial and generate vuggy, intragranular porosity that enhances reservoir quality and connectivity. Similarly aged Caddo mounds have been drilled in Stephens County just southeast and on the opposite flank of the Knox-Baylor Trough.

A forty-five foot core section was cut from the Rasberry Reef and tested for porosity, permeability and saturation content by Core Labs. Core-derived porosity ranges from 0.5% to 9.45% and bulk volume hydrocarbons ranges from 1.35% to 3.39%. Log-derived values derived using the Archie water saturation

equation and rock-fluid model are compared with core-derived values to identify and understand any discrepancies between the data sets.

Petrophysical logs are used to generate a rock-fluid model for the wells that displays their total porosity and rock matrix composition. The rock matrix model is built using photoelectric, bulk density and neutron-density porosity logs. Total porosity is represented as the sum of the bulk volume hydrocarbons, bulk volume water and clay bound water.

Seismic analysis used in conjunction with the material above provides the geologist with an understanding of the type of deposit and structure of the carbonate buildup, reservoir, and shelf margin. Once the structure is identified in cross section, instantaneous frequency attribute mapping is used to identify the lateral extent of porous reservoirs. Instantaneous frequency mapping identified several deltas deposited over different time periods that prograded over the surrounding reefs. The discoveries led to a new drilling program targeting a shelf edge reef and further evaluation of the carbonaceous deltas.

Table of Contents

Chapter 1: Introduction

Knox County, Texas is located in North-Central Texas near the Texas-Oklahoma border. The Knox-Baylor Trough is deposited here and covers a four county area including King, Haskell and Baylor County. Surrounding the Knox-Baylor Trough is the Red River Uplift, Electra Arch, Wichita Mountains, Muenster Arch, Ouachita Foldbelt, Concho Carbonate Platform and the Eastern Shelf (Figure 1).

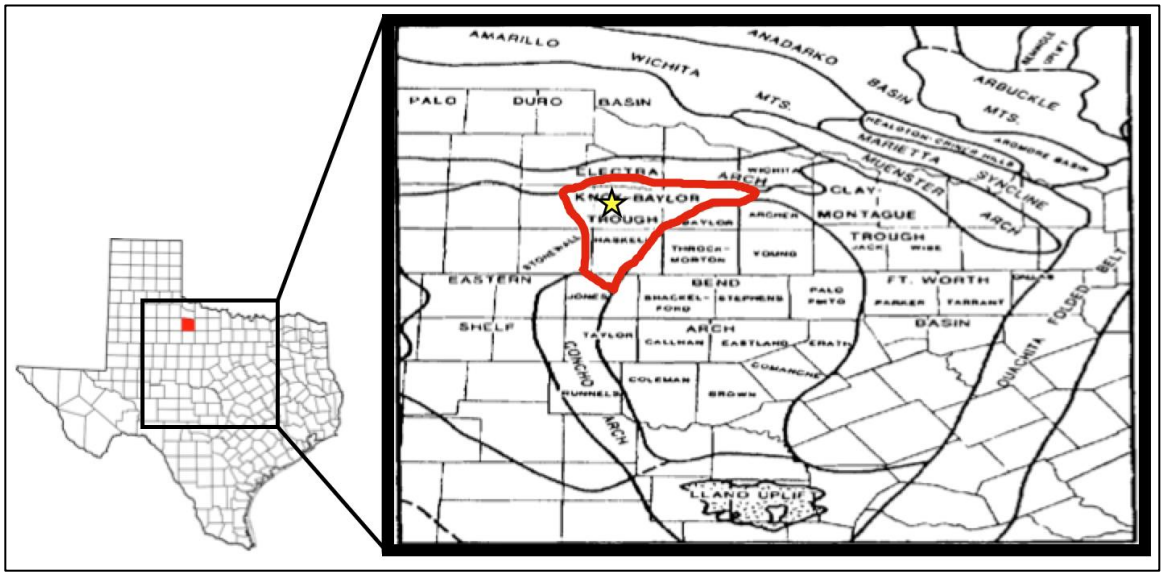

Figure 1. Map of Texas with Knox County highlighted in red. The extent of the Knox-Baylor Trough is outlined in red with yellow star denoting well locations (Flippen, 1982).

Knox County and the surrounding areas saw a combination of terrestrial, marginal-marine and carbonate sedimentation from the beginning of the Mississippian to the end of the Pennsylvanian. Sedimentation was controlled by eustatic sea level fluctuations caused by glacial icehouse conditions and regional

tectonic subsidence (Heckel, 1986). High frequency transgressive and regressive events are seen in well logs from the gamma ray and spontaneous potential logs. Stacking patterns from the gamma ray log are used to identify well-defined depositional cycles.

The primary reservoirs for the Wildcat Field are the Caddo Limestone and Rasberry Reef lithofacies. In the Knox-Baylor Trough, the Caddo Limestone is a mixed skeletal packstone to wackestone with phylloid algae and *Komia* bafflestone mounds. *Komia* is a type of red algae commonly found in mound buildups. The Caddo Limestone is deposited over a large area of North Central Texas and is associated with several shelf edge buildups (Johnson, 1961). Studies on Mississippian to Strawn aged reefs in North Central Texas have been published by numerous authors and are used to evaluate the Caddo aged Rasberry Reef carbonate mounds (Loucks and Fu 2016; Browning and Donovan 1989).

Tectonic History

In the early Paleozoic, Texas was a part of the southern leading edge of the North American continent (Figure 2). When the North American continent collided with the Gondwanaland continent, the Ouachita Foldbelt was emplaced on the eastern side of the Fort Worth Basin (Figure 3). The foldbelt activated subsidence in the Fort Worth Basin, surrounding regional troughs, as well as the Midland Basin. It was also a major sediment source during the Paleozoic (Cleaves, 1993).

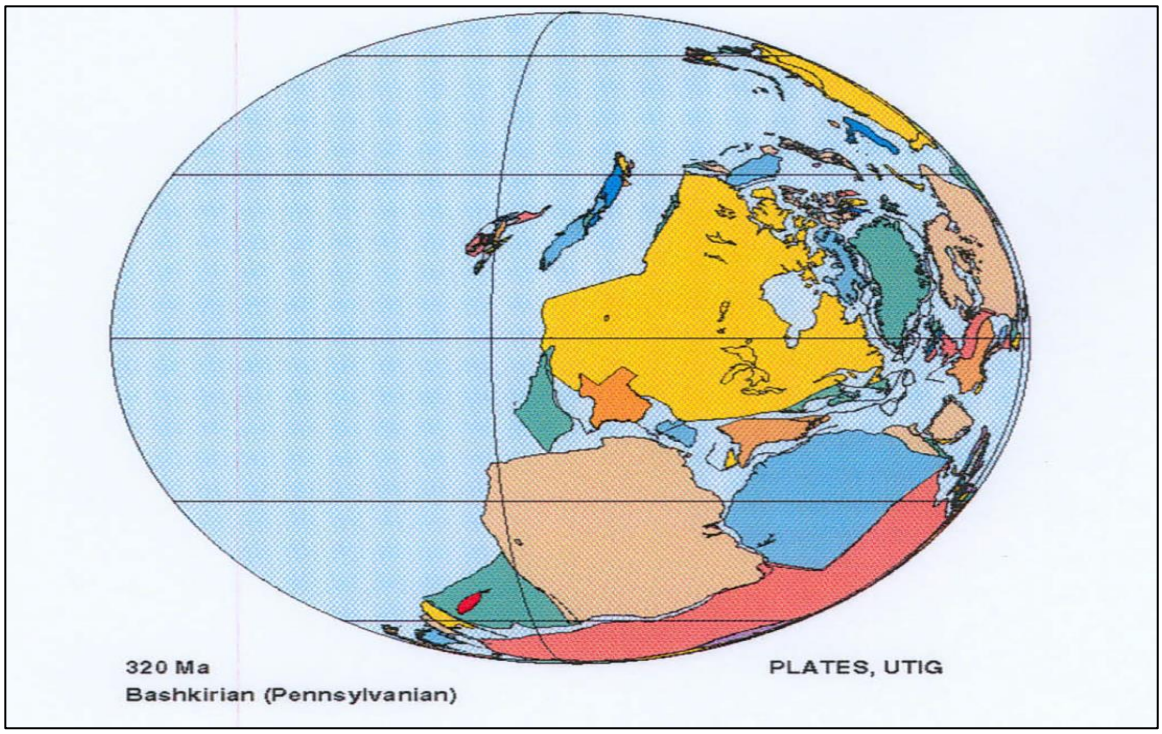

Figure 2. Pennsylvanian, North American plate tectonics (Dalziel et al. 2002).

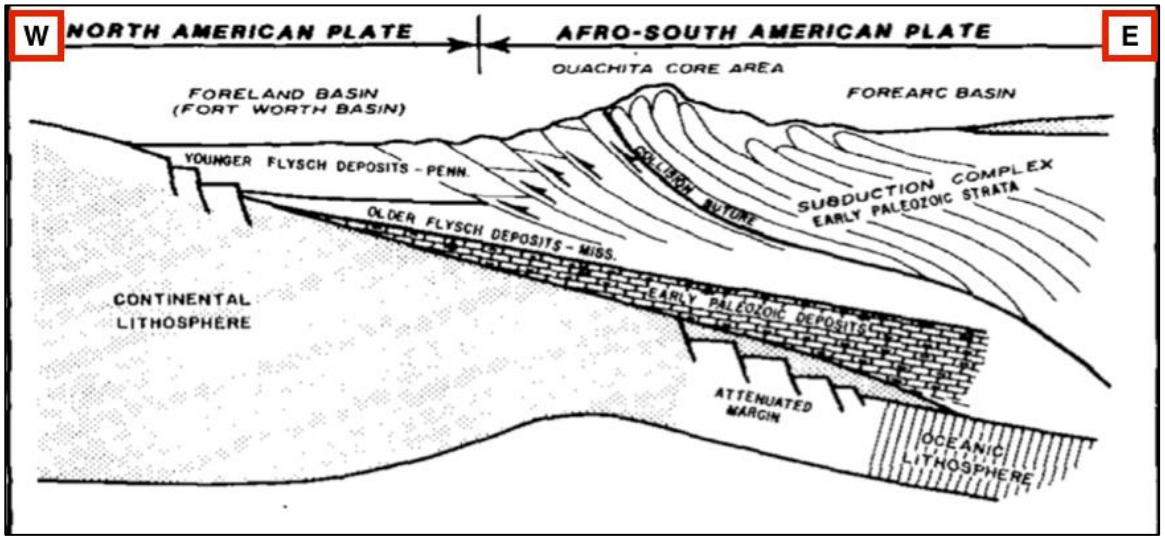

Figure 3. West-east cross section of the Fort Worth Basin and Pennsylvanian Ouachita Foldbelt (Walper, 1977).

Mississippian tectonics started with active subsidence of the preexisting Ellenburger carbonate platform followed by deposition of the Barnett Shale.

Secondary tectonic features were emplaced in the Morrowan and Atokan. These secondary features included the Electra Arch, Muenster Arch and Red River Uplift. The Electra Arch and Red River Uplift are important because of their proximity to the Knox-Baylor Trough. These structural highs were part of an east-west trending fault block. They were a terrestrial sediment source for the Fort Worth Basin and a stable site of deposition for carbonate platforms and shelf edge buildups like the Caddo limestone (Cleaves and Erxleben, 1983). The beginning of the Desmoinesian was marked by accelerated subsidence. Subsidence in the Fort Worth Basin and surrounding Knox-Baylor and Clay-Montague troughs helped form the broad arch of the Concho Platform. Subsidence slowed in the late Desmoinesian allowing the progradation of deltas onto the Concho Platform. Missourian deposition marks the initiation of subsidence in the Midland Basin and Eastern Shelf. As the Eastern Shelf developed its slope system and the Ouchita foldbelt continued to advance, westward progradation of deltas and fluvial deposits followed.

Depositional History and Stratigraphy

As noted earlier, high frequency transgressive and regressive events created the complex stratigraphic record of North Central Texas (Figure 4). From the Ordovician to the Mississippian, carbonates and mudstones were deposited across a passive continental margin. When seas regressed and basin depocenters were formed by active subsidence, Atokan to Pennsylvanian carbonates and clastics were deposited (Figure 5). The Knox-Baylor Trough formed as a pathway for sediments from the surrounding areas to be transported

to the Permian Basin (Gunn, 1979). As deltas from structural highs migrated with regressive seas at the end of the Pennsylvanian, clastics were deposited over preexisting carbonate platforms and shelves and transported to the Permian Basin (Pollastro et al, 2007).

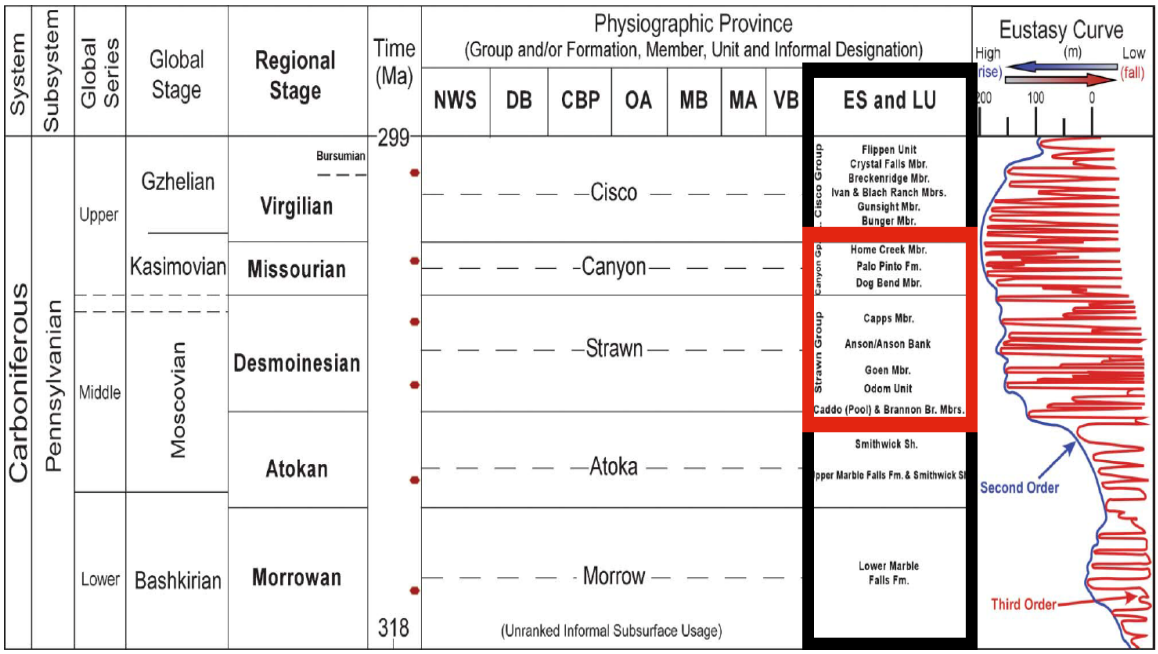

Figure 4. Pennsylvanian stratigraphic column with the Eastern Shelf (ES) and Llano Uplift (LU) section outlined in black. Study interval outlined in red (Wright, 2011).

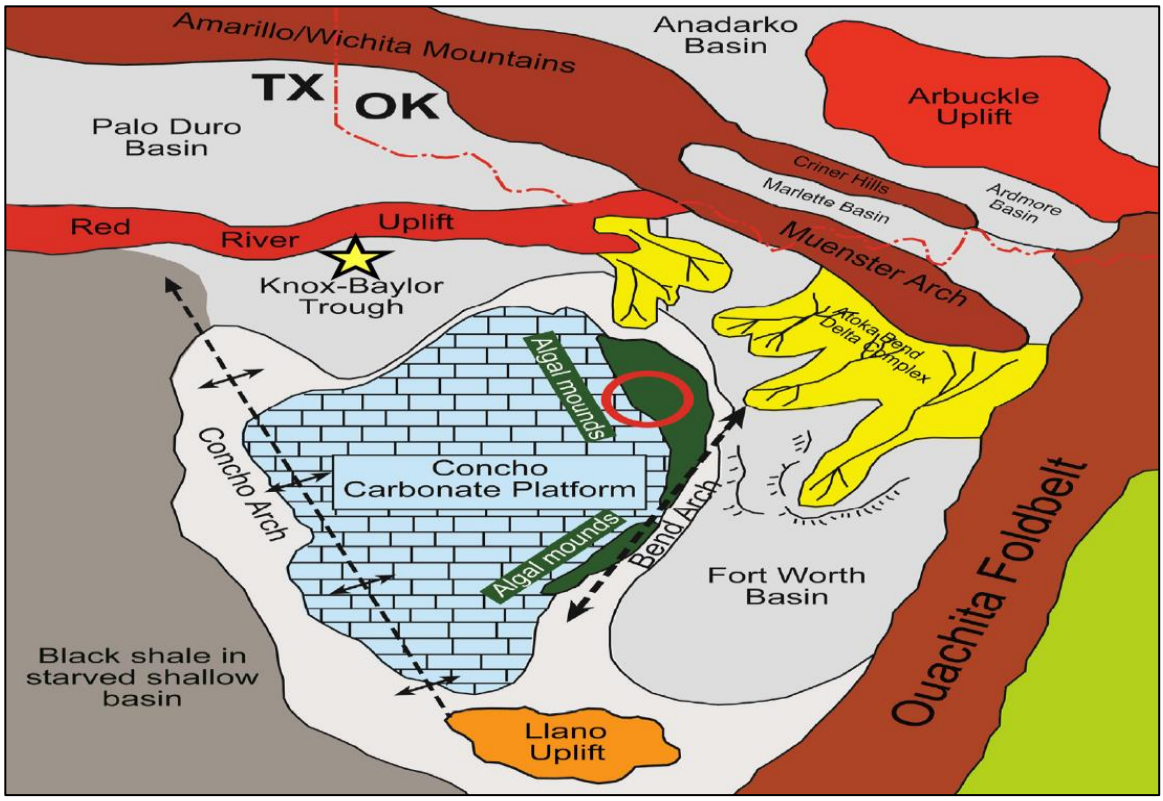

Figure 5. Paleogeographic map of the Desmoinesian with yellow star denoting well locations (Loucks and Fu, 2016).

For this study, the stratigraphic record from the Ellenburger to the Canyon is marked on well logs and seismic section. The Ellenburger Group was deposited in the early Ordovician as an epeiric carbonate platform that covered a large part of Texas. A drop in sea level during Ordovician exposed the Ellenburger creating a karst surface in its upper section (Sloss, 1988). Mississippian deposition followed with alternating limestone and phosphatic black shales. As the Ouachita foldbelt was emplaced in the early Mississippian and subsidence began, more accommodation space became available for deposition of the Meramecian aged Barnett Shale. The Concho Platform formed during the Pennsylvanian as a rimmed platform with a well defined shelf edge and slope

system. Phylloid algal mounds accumulated on the platform's shelf edge (Figure 5). Five major deltas formed in North-Central Texas during the Pennsylvanian: Bowie, Perrin, Haskell, Henrietta and Eastland (Cleaves, 1993). The Haskell Delta cuts through Knox County and fed the Knox-Baylor Trough (Figure 6). The late Pennsylvanian saw these deltas prograde across the Concho Platform to the Eastern Shelf and Permian Basin as seas regressed.

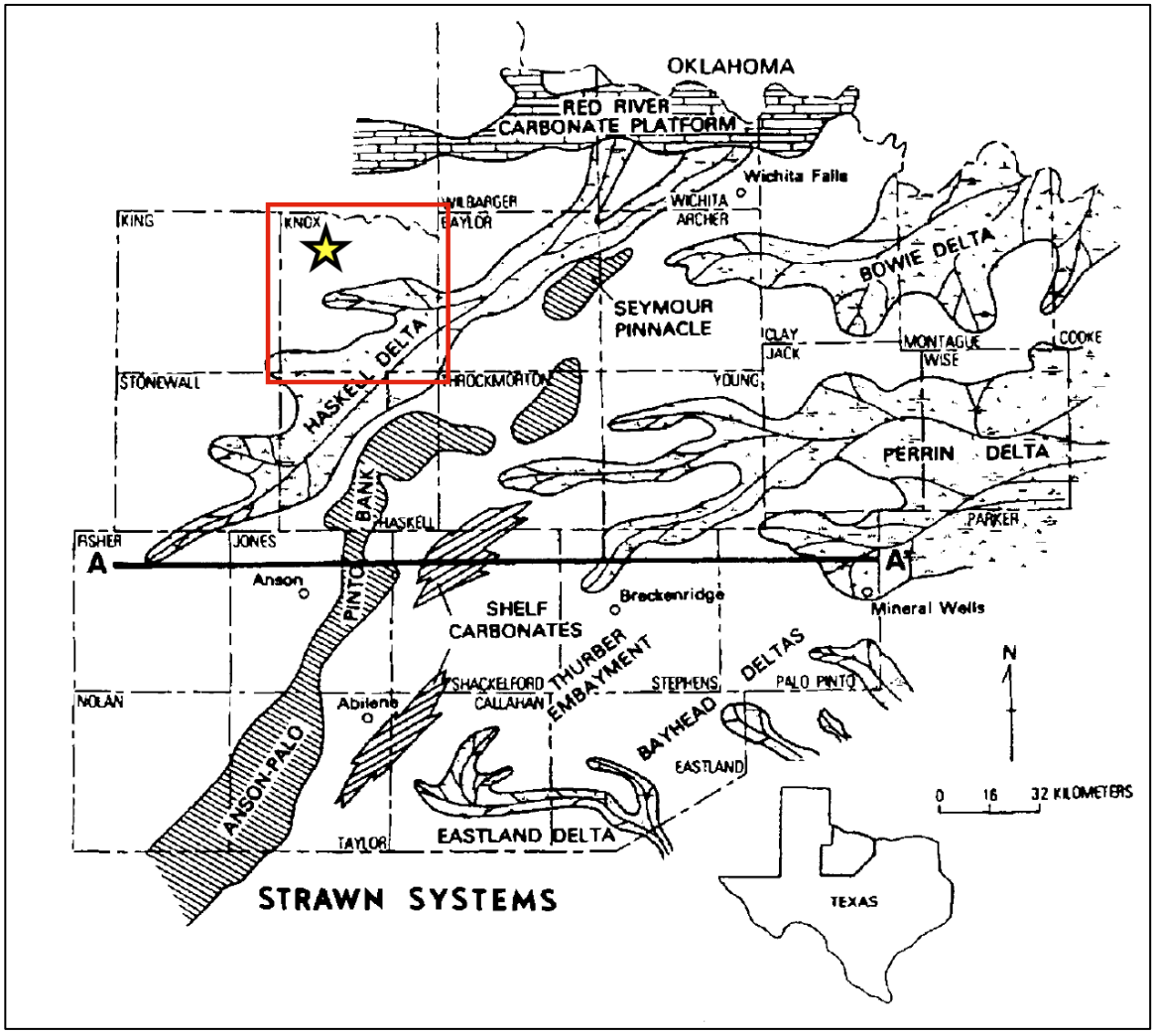

Figure 6. Strawn depositional environment with a yellow star denoting the well location of 9 wells used in this project (Cleaves, 1993).

Caddo Phylloid Algal Shelf Edge Buildups

The data for this thesis comes from a Caddo phylloid algal mound. In North Central Texas, phylloid algal mounds have been drilled in Stephens, Palo Pinto and other counties around the Concho Platform shelf edge. Mounds produce from the Mississippian up to the Caddo. This thesis will focus on Caddo aged phylloid algal mounds.

High relief carbonate mounds are defined as being greater than sixteen feet tall with large, lenticular deposits of wackestone to grainstone (Riding, 2001). They accumulate during rising sea levels on deepwater carbonate platforms and are molded by ocean currents (King, 1990). They grow by a process called sediment baffling (Figure 7). Sediment baffling involves stalked crinoids and fenestrate bryozoans acting as a baffle and trapping mechanism for organic muds transported by ocean currents. Laudon and Bowsher claimed that the organic mud accumulation may have been self localized and accumulated by on mound sediment producing algae (Laudon and Bowsher, 1941).

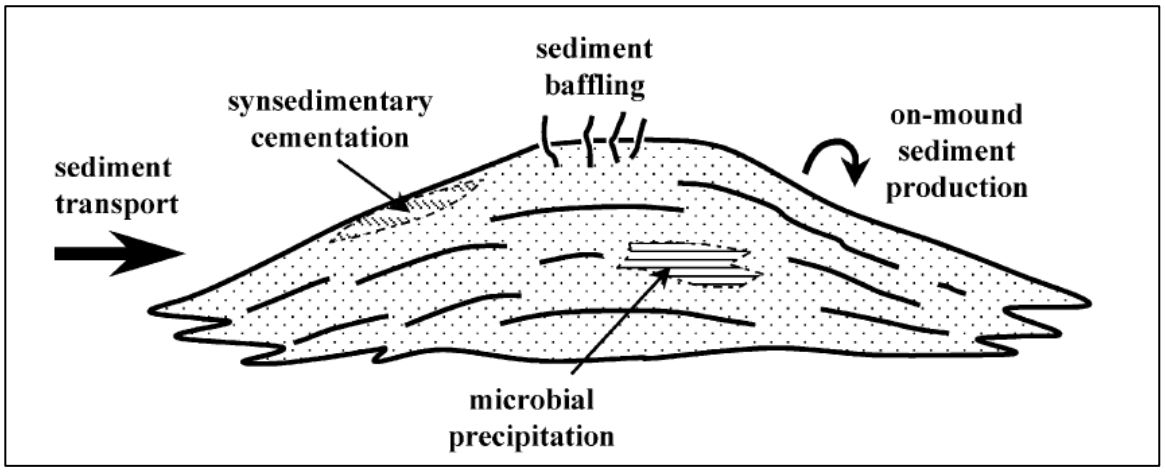

Figure 7. Carbonate sedimentation mechanisms (Riding, 2001).

In Stephens County, multiple papers have been written on Caddo phylloid algal mounds. There is no single model for carbonate mounds, as they have varying carbonate composition, depositional environments, and porosity. Loucks and Fu (2016) present three different depositional models for Caddo phylloid algal mounds based on relative sea level (Figure 8).

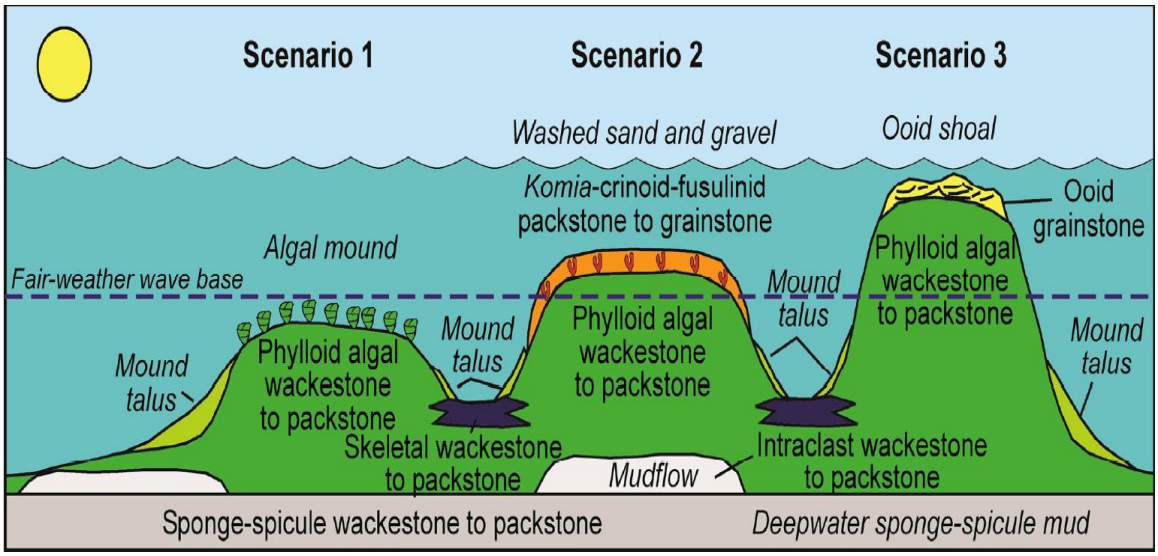

Figure 8. Caddo phylloid algal mound depositional models (Loucks and Fu, 2016).

In scenario 1, bafflestones form the main core of the mound and trap sediments transported in by ocean currents and debris flow. Scenario 1 is found during highstand deposition. As sea level begins to fall in the later part of the highstand systems tract, scenarios 2 and 3 become more abundant. Scenario 2 involves the wackestone to packstone mound being deposited just above a fair-weather wave base and has the mound being shoaled by a *Komia*-fusulinid-crinoid sand transported from a high relief area. Scenario 3 is found just prior to subaerial exposure and has a cross-bedded ooid capping sandstone. Scenario 3 has the highest energy of the three environments. The mound talus is a low

energy intermound area that contains phylloid algae, *Komia*, crinoid and bivalve fragments shed off the mound or transported in (Loucks and Fu, 2016).

Diagenesis is the main control on porosity development in the mounds. Figure 9 shows the timing of diagenesis and the various mechanisms for porosity development and cementation. Understanding the depositional environment is important because the grain dissolution and precipitation is tied to specific environments. To determine the environment, observation of pore structure and composition is necessary. The Knox-Baylor Trough had a large volume of sediment transported in and also had high frequency transgressive and regressive events. This presents the opportunity for multiple depositional environments that may include rapid burial, subaerial exposure, meteoric water exposure and more that may affect diagenesis.

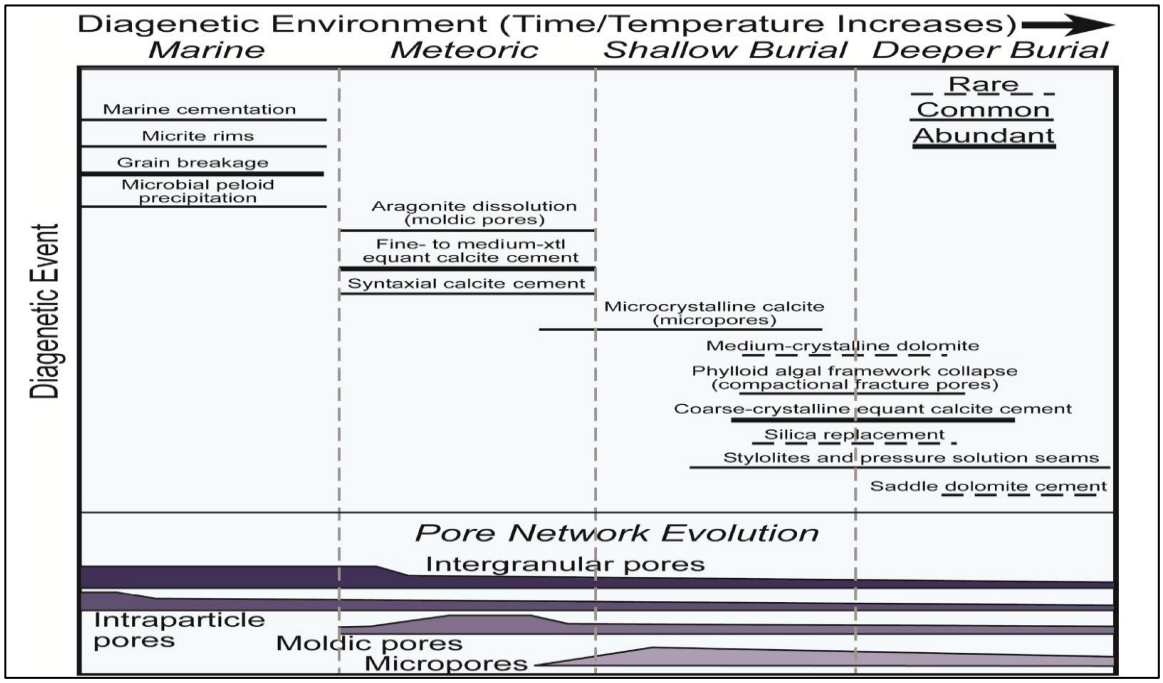

Figure 9. Diagenesis chart of Caddo limestones and their pore network evolution (Loucks and Fu, 2016).

Phylloid algal mounds can be identified in seismic section by a reflector sag (Figure 10; Browning and Donovan, 1989). A reflector sag is caused by contrasting stacking velocities from shales and dense carbonates. Accumulated material from sediment baffling creates a dense carbonate deposit that affects the overlying and underlying layers.

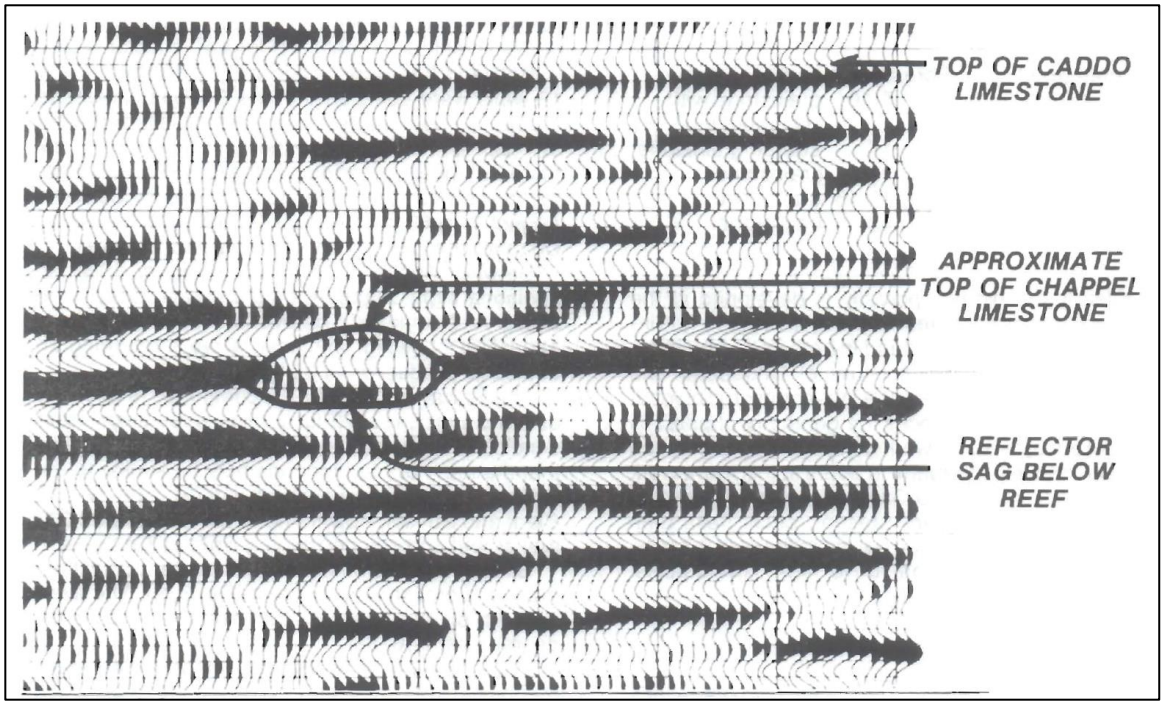

Figure 10. Mississipian and Caddo reefs with reflector sags from Stephens County, TX (Browning and Donovan, 1989).

Previously Studied Phylloid Algal Mounds

Pennsylvanian phylloid algal mounds have been drilled in Utah, New Mexico, Oklahoma and Texas. The mounds display similar depositional and lithostratigraphic properties. Mounds are deposited in moderate energy, open-marine environments on a shelf or shelf break. Deposition can be tidal or wave

oriented. Tidal oriented mounds trend in the dip direction and wave oriented mounds trend in the strike direction (Grammer and Ritter, 1996).

The mounds have variable sizes and stacking patterns. In the Paradox Basin of southeast Utah, Pennyslvanian mounds are 10’ to 45’ high and 115’ to 165’ wide. The mounds coalesce together as they aggrade upwards forming mound complexes 1000’ to 1300’ long. Mounds are spaced 100’ to 230’ apart. In the Anadarko Basin of northwest Oklahoma, Oswego Limestone mounds are deposited off the Northern Shelf. Oswego Limestone mounds are approximately 125’ high. Progradational stacking of mounds precedes retrogradational stacking here (Geary, 2008).

To the southeast of Knox County, Desmoinesian, Caddo phylloid algal mounds are deposited in Stephens County. These mounds were deposited at the same time as the Rasberry Reef mounds and are directly related. The Caddo mounds are deposited on the shelf edge of the Concho Platform. The mounding cycle consists of deepwater, mound base, mound core, intermound, and capping lithofacies. The mound core consists of a phylloid algal bafflestone to wackstone lithofacies (Browning and Donovan, 1989).

Chapter 2: Hypotheses

The Knox County Rasberry Reef phylloid algal mound has reservoir properties matching Pennsylvanian aged mounds deposited on the Concho Platform. Porosity in the mound is tied to carbonate type and diagenesis, and the best reservoir as determined from well logs is found in the phylloid algal bafflestone mound. The mound has an identifiable structural trend on the

Rasberry Reef isopach map that can be used to locate similar mounds and reefs in the area. Mounding cycles are identifiable in well logs using the spontaneous potential log.

Seismic attributes are used in conjunction with porosity and resistivity logs. The instantaneous frequency attribute is used to identify porous fracture zones, lithology variations, and hydrocarbon bearing zones.

Chapter 3: Data

Loudon Exploration based out of Dallas, TX provided the data for this thesis. Loudon Exploration operates 9 wells that produce from Caddo to Strawn aged reefs in Knox County. Well logs, 3-D seismic and core are used for this study.

Well logs with LAS files are available for all 9 wells. Gamma ray, spontaneous potential, photoelectric, bulk density, porosity and resistivity logs are found in the LAS files. Log aliases for porosity and resistivity logs are shown in Table 1. LAS files are uploaded into Petra software.

Table 1. Log aliases for bulk density, porosity, and resistivity logs for 9 wells.

	PFER 1	Ellis Ranch 1	Ellis Ranch 2	Ellis Ranch 3	Ellis Ranch 4	Ellis Ranch 5	Ellis Ranch 6	Ellis Ranch 7	Ellis Ranch 8
API	4227532307	4227532272	4227532282	4227532283	4227532287	4227532296	4227532298	4227532318	4227532323
Kelly Bushing	1389	1461	1479	1453	1450	1433	1491	1408	1455
Total Depth	9000	6050	5905	5854	5886	5868	5912	6096	6400
SFL	RT30	AF10	SFL	SFL	SFL	AF10	AF10	AF10	AF10
ILM	RT30	AF30	ILM	ILM	ILM	AF30	AF30	AF30	AF30
ILD	RD	AF90	ILD	ILD	ILD	AF90	AF90	AF90	AF90
RHOB	RHOB	RHOZ	RHOB	RHOB	RHOB	RHOZ	RHOZ	RHOZ	RHOZ
NPLS	NPHI	NPHI	NPLS	NPLS	NPLS	NPHI	NPHI	NPHI	NPHI
DPHZ	DPHZ	DPHZ	DPLS	DPLS	DPLS	DPHZ	DPHZ	DPHZ	DPHZ

Tidelands Geophysical shot the 27 mi^2 3-D vibroseis program (Figure 11). Three vibroseis vehicles performed four sweeps with twelve-second sweep

lengths and two-second listen times. Acquisition used 18 lines by 68 reclines and was processed to 82.5’ by 165’ bins. The SEGY files were uploaded into Kingdom IHS software with regional wells.

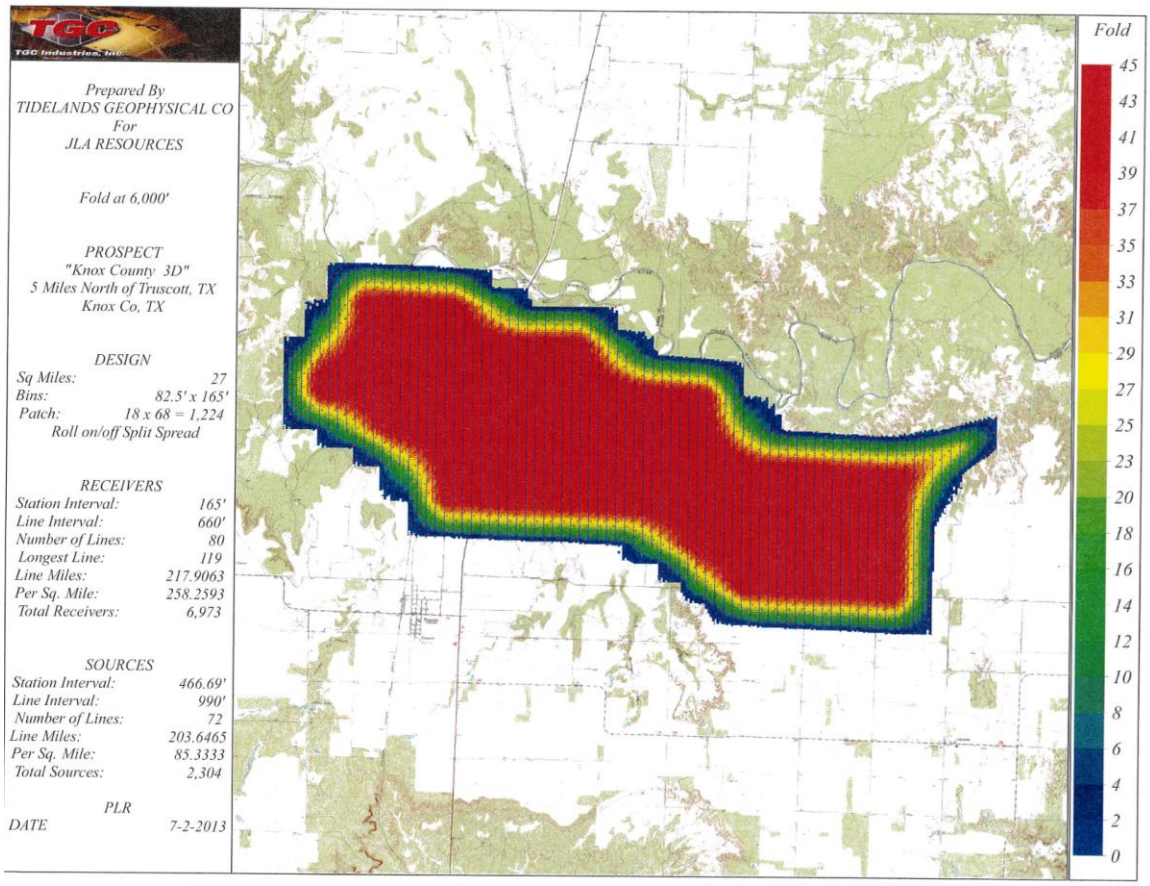

Figure 11. Tidelands Geophysical 3-D seismic program for Loudon Exploration.

Ellis Ranch 2 had a 45’ section of core cut from the Rasberry Reef interval. The upper depth is located at 5697’ and the lower depth is located at 5741’. Core plugs were taken at 1’ intervals from the 45’ core section and sent to Core Labs for analysis. Core Labs measured permeability, porosity, bulk density, and pore volume saturations. In addition, Dravis Geological Services was contracted by Loudon Exploration to describe the core lithology, prepare thin sections and analyze diagenetic properties.

Chapter 4: Methods

Log Interpretation and Petrophysical Evaluation

Rock-Fluid Model

Logs and log-derived values are used to build the rock-fluid model, correlate core and log derived values, and identify zones of interest within the data set. The rock-fluid model takes log measurements and displays them as reservoir properties for prospect evaluation. Gamma ray, resistivity, and porosity logs are used in the following equations to build the model and present the data in a manner appropriate for reservoir characterization and prospect evaluation.

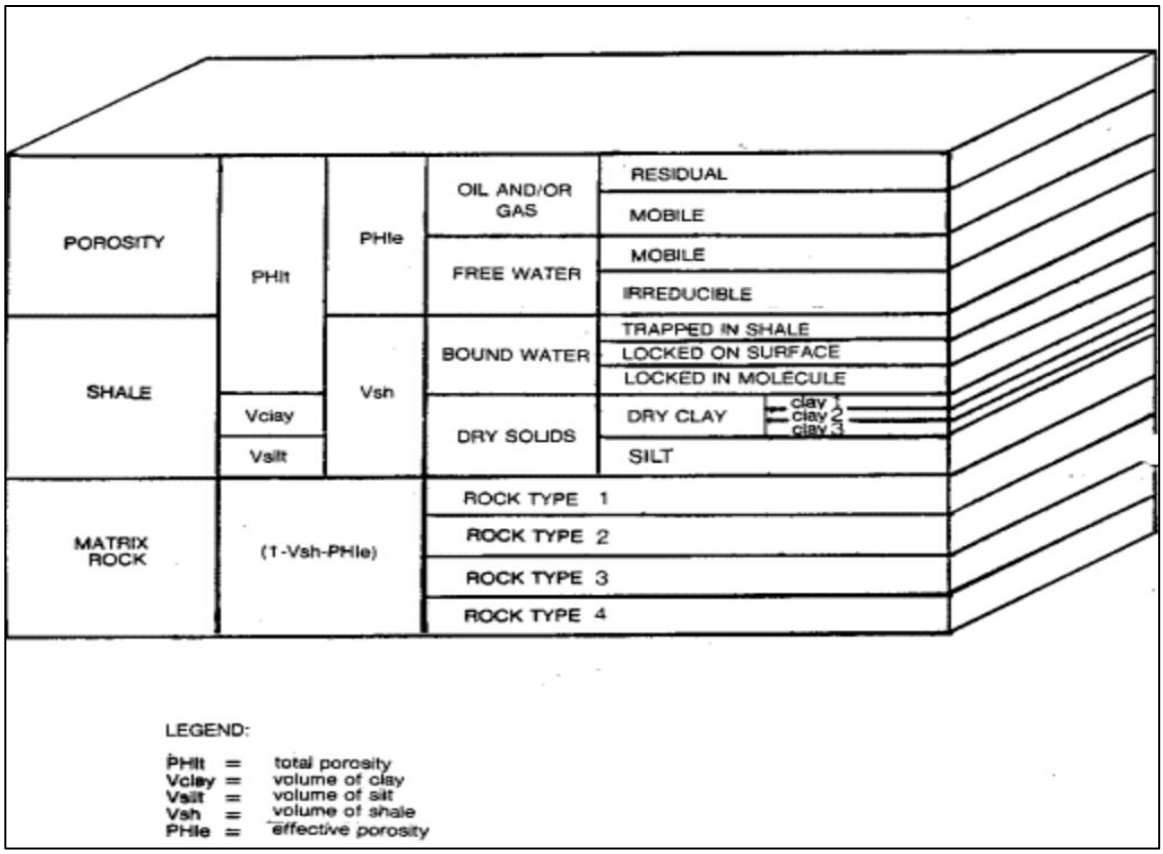

Figure 12. The rock-fluid model (Crain, 1978).

Gamma Ray Log

Shale volume is derived from the gamma ray log. The first step in calculating the shale volume is to determine the gamma ray index, I_{GR}, which is a linear model for shale volumes. Gamma ray values defining carbonate, GR_{min}, and shale intervals, GR_{max}, are determined from a histogram of the gamma ray data. Carbonate intervals are defined by the bottom 5% of gamma ray values and shale intervals are defined by the top 5% of gamma ray values (Asquith and Krygowski, 2004). The nonlinear Steiber model, V_{sh}, is used to determine the shale volume in the rock-fluid model (Steiber, 1970).

Eq. 1
$$I_{GR} = \frac{GR_{\log} - GR_{\min}}{GR_{\max} - GR_{\min}}$$

Eq. 2
$$V_{sh} = \frac{I_{GR}}{3 - 2 \times I_{GR}}$$

Porosity Logs

Neutron porosity, *NPLS*, and density porosity, *DPHZ*, logs are used to approximate the total porosity, Φ_T, for a non-gas reservoir. The effective porosity, Φ_{eff}, is then determined from a product of the total porosity and relative shale volume (Crain, 1978). The total porosity for the rock-fluid model is shown in track 4 as the sum of the bulk volume hydrocarbons, clay bound water and bulk volume water.

Eq. 3
$$F_T = (DPHZ + NPLS)/2$$

Eq. 4
$$F_{eff} = F_T \times (1 - V_{sh})$$

Archie's Water Saturation

The water saturation of a reservoir's uninvaded zone, S_w, is determined from the Archie equation (Archie, 1942). Representative values of the tortuosity constant, *a*, cementation exponent, *m*, and saturation exponent, n, for carbonate intervals are 1, 2 and 2 respectively (Archie, 1942; Asquith, 1980). The deep resistivity log, *ILD*, was used to approximate the formation's true resistivity, R_t. The resistivity of formation water at formation temperature, R_w, can vary widely between formations and lead to large discrepancies in water saturation and bulk volume water. A standardized value of 0.035 ohms was used based on a calculated R_w from a water sample in the Ellis Ranch 2 Rasberry Reef section.

Eq. 5
$$S_w = \left[\frac{a \cdot R_w}{R_t \cdot \phi^m}\right]^{\frac{1}{n}}$$

Bulk Volume Water

Bulk volume water, *BVW*, is the product of the formation's water saturation and effective porosity. It is a good indicator of a water free completion. When bulk volume water is constant within a formation it means the formation is at irreducible water saturation. A formation is said to be at irreducible water saturation when water in the uninvaded zone does not migrate and is held on the grains by capillary pressure (Morris and Biggs, 1967). *BVW* values for carbonates are listed in Table 2. *BVW* values increase with decreasing grain size because the volume of water a formation can hold by capillary pressure increases with decreasing grain size (Asquith and Krygowski, 2004).

Eq. 6
$$BVW = \phi_{eff} \cdot S_w$$

Table 2. Bulk volume water values for different carbonate porosities (Asquith and Krygowski, 2004).

Carbonate Type	Bulk Volume Water
Vuggy	0.005 to 0.015
Vuggy and Intergranular	0.015 to 0.025
Intercrystalline	0.025 to 0.04
Chalky	0.05

Clay Bound Water

Clay bound water, *CBW*, is the product of the bulk volume water and the shale volume. Clay bound water represents the volume of water trapped in a shale, held on a shale by capillary pressure, and bonded to other molecules within the shale (Crain, 1978).

Eq. 7 $$CBW = BVW \acute{} \ V_{sh}$$

Matrix Identification Plot (U_{maa} v ρ_{maa})

The photoelectric log, *Pe*, is measured in barns per electron and is a good indicator of a formation's lithology (Dewan, 1983). When used in conjunction with the bulk density log, ρ_b, and the neutron-density porosity log, Φ_{ND}, *Pe* is used to determine a formation's apparent volumetric cross section, U_{maa}. The apparent volumetric cross section is measured in barns per cubic centimeter. The photoelectric absorption of fluid, U_{fl}, is 1. Common values for three different lithologies observed in the data set are shown in Table 3.

Table 3. Apparent matrix values for common minerals (Asquith and Krygowski, 2004).

Lithology	ρ_{maa} (g/cm^3)	Δt_{maa} (µsec/ft)	U_{maa} (barns/cm^3)
Sandstone	2.65	55.5	4.78
Limestone	2.71	47.5	13.8
Dolomite	2.87	43.5	8.98

To display the rock-fluid model in track 5, the calculated apparent volumetric cross section log is plotted with clay bound water, effective porosity, shale volume, and neutron-density porosity. Using the lithology summary tool in Petra, shading crossovers are assigned to accurately display rock and fluid volumes. When the neutron-density porosity log is greater than the apparent volumetric cross section log, sandstone is indicated (Asquith and Krygowski, 2004).

Eq. 8
$$U_{maa} = \frac{(Pe \cdot \rho_b) - (\phi_{ND} \cdot U_{fl})}{1 - \phi_{ND}}$$

Permeability

Log-derived permeability calculations require the formation to be at irreducible water saturation to accurately predict permeability. If the formation is not at irreducible water saturation, then log-derived values will not be a good estimate of a formation's permeability. Equation 9 uses the effective porosity and water saturation of the flushed zone to determine permeability (Timur, 1968).

Eq. 9
$$K = \left[\frac{93 \cdot \phi_{eff}^{2.2}}{S_{xo}}\right]^2$$

Log Crossplots

Log crossplots graphically display log values to estimate rock properties such as lithology. Two lithology crossplots are generated to determine rock types and volumes. The neutron-density crossplot plots the neutron porosity log, *NPLS*, against the bulk density log, *RHOB*. It is used to plot lithology in a three-component system. Lithology lines are superimposed on the plot to determine lithology and porosity. One problem with this crossplot is determining which lithology is dominant when the point plots between two lithology lines. Applying core observations and regional lithology trends will help reduce the discrepancy in lithology approximations. The matrix-identification crossplot plots the apparent volumetric cross section, U_{maa}, against the apparent grain density, ρ_{maa}. This crossplot is used to determine rock matrix composition in a four-component system. The apparent volumetric cross section is measured in barns per electron and is calculated from the photoelectric log, bulk density log, neutron-density porosity log, and photoelectric absorption of fluid.

Buckles plots are used to support bulk volume water calculations (Asquith, 2004). The Buckles plot displays effective porosity against Archie water saturation. Hyperbolic curves representing bulk volume water concentration are overlain on the chart. When points plot along the same hyperbolic curve, the formation is at irreducible water saturation. If the data points are scattered the formation is not at irreducible water saturation and water is expected to produce with hydrocarbons.

Core Analysis

Three core thin sections were selected from the Ellis Ranch 2 forty-five foot core section for description and analysis based on petrophysical reservoir quality. Calculated porosity, permeability and bulk volume hydrocarbons were used to select thin sections for detailed analyses. The thin sections were described based on their name, fossil abundance, pressure solution, cements, associated minerals, and depositional environment (Dunham, 1962).

The thin sections provided by Dravis Geological Services were oriented in the z or upwards direction and prepared by staining one-half of each thin section with dual carbonate stain, Alizarin Red S and potasssium ferricyanide (Dickson, 1965). When used together the stains differentiate calcite from dolomite and reveal iron-rich varieties of the two-carbonate lithologies. Thin sections were looked at under standard and diffused plane-polarized light (Dravis and Yerwicz, 1985; Wendte, et al., 1998). The diffused plane-polarized light technique can identify diagenetic fabrics and secondary microporosity that would otherwise be difficult to identify under plane-polarized light.

After the thin sections have been described, core and log derived porosity, permeability, bulk volume hydrocarbon and bulk volume water values are compared for Ellis Ranch 2. Values are taken at an interval of every foot. The values are used to describe reservoir quality within the deeper subtidal, off-mound debris, mound and mound base sections of the Rasberry Reef carbonate mound. Standard error values are calculated to determine the reliability of the log derived values.

Seismic Analysis

Seismic data measures in two-way time the time it takes for a wave generated from a source to travel to subsurface strata and back to receivers on the surface. Three models will be generated from the 3D seismic data set: time, velocity, and depth. The goal of these models is to accurately build a model of the depth and subsurface structure.

Before any horizons are picked or formation tops input, stacking velocities go through the dip moveout process and dip moveout stacking velocity analysis to generate a poststack migration time. This is the first step in building the time model (Herron, 2011). Horizons are picked based off of zero crossing wavelets between contrasting layers and a grid is applied to the picks to generate a continuous time event.

Once horizons are picked and gridded, formation tops made in Petra are uploaded to the wells in Kingdom. Formation tops are input as true vertical depth. Kingdom's dynamic depth conversion tool will build the last two models. The best model assumes the strata are near horizontal and of equal thickness. This is not always the case though. The model computes the interval velocity for a formation from formation tops and picked horizons. If the formation is not isotropic and homogenous, the velocity and depth model may be inaccurate.

Eq. 10 $$V_{\text{int}} = 2\Delta Z / \Delta t$$

Eq. 11 $$Z_{top} = T_{top} \times V_{\text{int}}$$

Time, (ms)	Depth, (feet)	Kingdom Model
Δt1	ΔZ1	Vint1=(2×ΔZ1)/Δt1
Δt2	ΔZ2	Vint2=(2×ΔZ2)/Δt2
Δt3	ΔZ3	Vint3=(2×ΔZ3)/Δt3

Figure 13. Velocity Model (Herron, 2011).

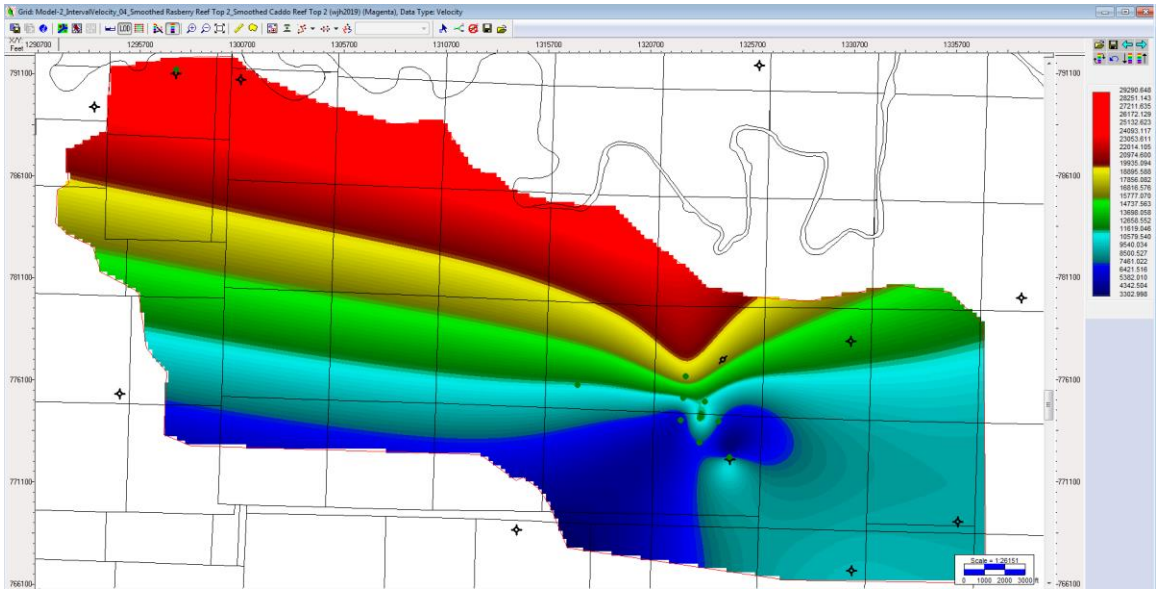

Figure 14. Interval Velocity Rasberry Reef

Seismic Attributes

Based on seismic data, seismic attributes can be used to identify differences in lithology, fracture zones, hydrocarbon zones and lateral variations in porosity amongst other measurements. The instantaneous frequency will be used here.

The instantaneous frequency attribute is the time derivative of the phase or the rate of change of the phase (Sarhan, 2017). It is an indicator of bed thickness, lithology variations, fracture zones and hydrocarbons. Low frequency readings are associated with unconsolidated layers like porous sands and fracture zones. High frequency readings are associated with dense shales and carbonates.

Chapter 5: Results

Thin Sections

The three observed thin sections follow Loucks's and Fu's scenario two depositional model for Caddo, phylloid algal mound complexes. The scenario two model has a phylloid algal bafflestone to packstone mound lithofacies with a draping *Komia*, packstone to grainstone lithofacies (Loucks and Fu, 2016). Based on the observed core, thin sections and well logs, two reservoirs are represented by the sample from 5701.7' and the samples from 5717.1' and 5729.3' (Table 4).

Table 4. Core plug measurements.

Depth (ft)	Porosity (%)	Permeability (md)	BVH (%)
5701.7	11.0	1.76	3.93
5717.1	14.4	243	4.48
5729.3	13.0	57.0	3.64

The reservoir found at 5701.7' has a porous, *Komia* packstone to wackestone lithofacies. The allochems seen in this lithofacies include crinoids, brachiopods, bryozoans, *Komia*, foraminifers, molluscs, and peloids. The allochems are associated with deeper subtidal and open-marine environments.

Based off the range of allochems, the mound may have been deposited in a draping or intermound area. Diagenesis occurred during shallow and deep burial and may not have experienced any subaerial exposure to meteoric waters. Calcite cement with sporadic accumulations of kaolinite are present. Vuggy and intraparticle porosity are the most abundant pore types. Numerous stylolites are present throughout the sample. The stylolites may have acted as a pathway for the flow of diagenetic fluids that generate vuggy porosity (Figure 15).

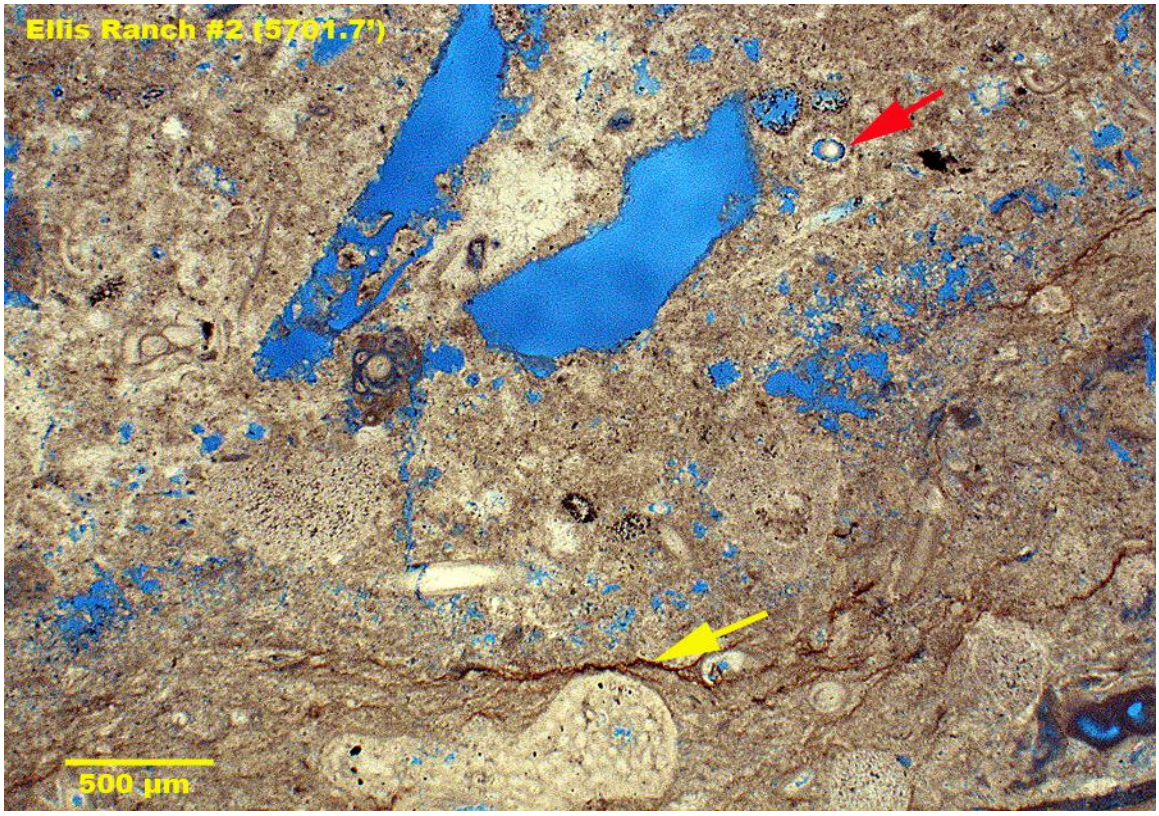

Figure 15. Thin section from 5701.7' viewed under diffused plane-polarized light. Stylolites are present in the lower (yellow arrow) and upper right areas. Vuggy and intraparticle porosity (red arrow) are common.

The reservoir found at 5717.1' has a dolomitic, mixed skeletal packstone lithofacies. Phylloid algae are abundant in this sample. Secondary allochems

present in the sample include crinoids, bryozoans, brachiopods, *Komia*, intraclasts and ostracods. The allochems are associated with an open-marine environment occurring below the fair-weather wave base. The sample comes from the top of the phylloid algal mound. The sample has a higher content of lime mud and marl reflecting the deeper depositional environment. Diagenesis occurred during deep burial. Two indicators of this are the occurrence of fracture pores and stylolites. Fracture and moldic pores are tied to the dissolution of the phylloid algae framework (Figure 16). Stylolites are found with vuggy pores.

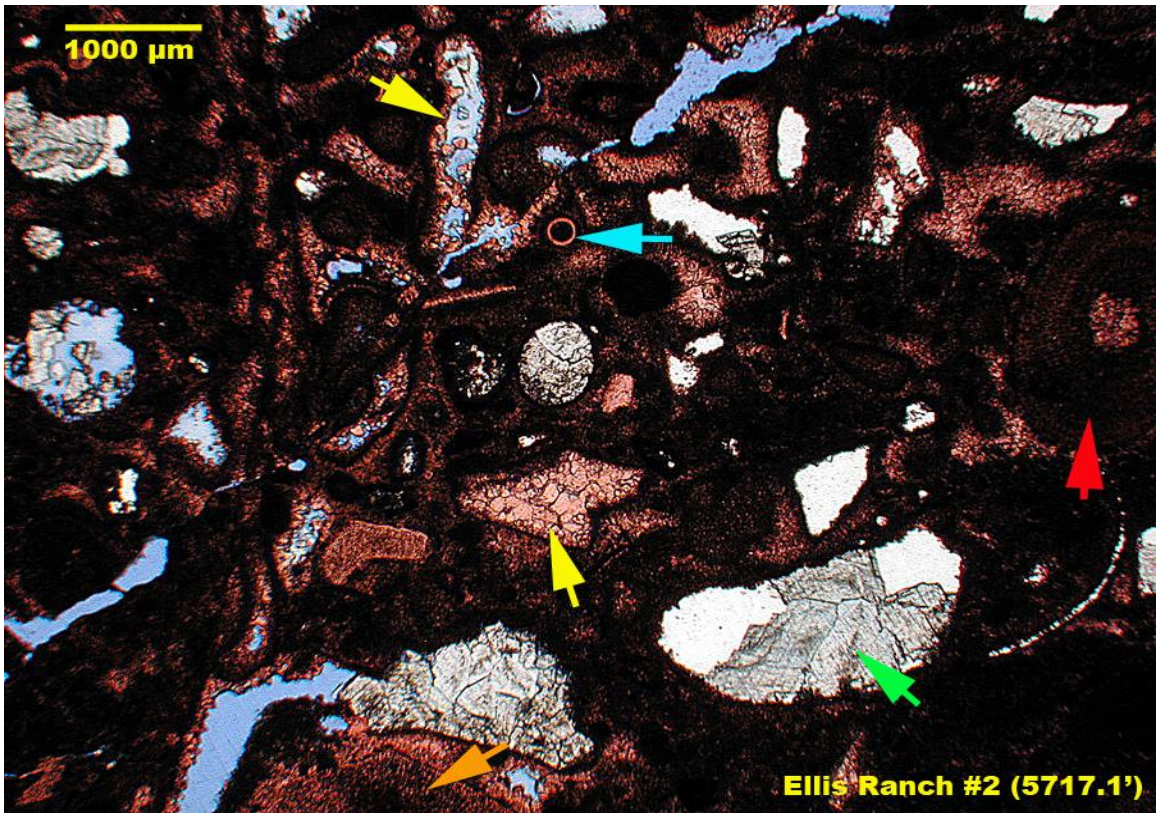

Figure 16. Thin section from 5717.1' viewed under plane-polarized light. Formation of saddle dolomites (green arrow) followed dissolution of aragonitic phylloid algal grains (yellow arrow). *Komia* (red arrow), crinoids (orange arrow) and calcispheres (blue arrow) are present.

The reservoir found at 5729.3’ has a porous, dolomitic, phylloid algal bafflestone lithofacies (Figure 17). Allochems present include crinoids, bryozoans, ostracodes, calcispheres, *Komia*, rugose corals and molluscs. The allochems are associated with an open-marine environment occurring below the fair-weather wave base. The sample comes from the basal section of the phylloid algal mound. Diagenesis occurred during deeper burial as noted by the occurrence of stylolites and dissolution of phylloid algal grains followed by dolomite recrystallization. The sample had a high concentration of original marine cement and intraparticle porosity was preserved throughout a large part of the sample. The primary porosity is specifically tied to the dissolution of phylloid algal grains.

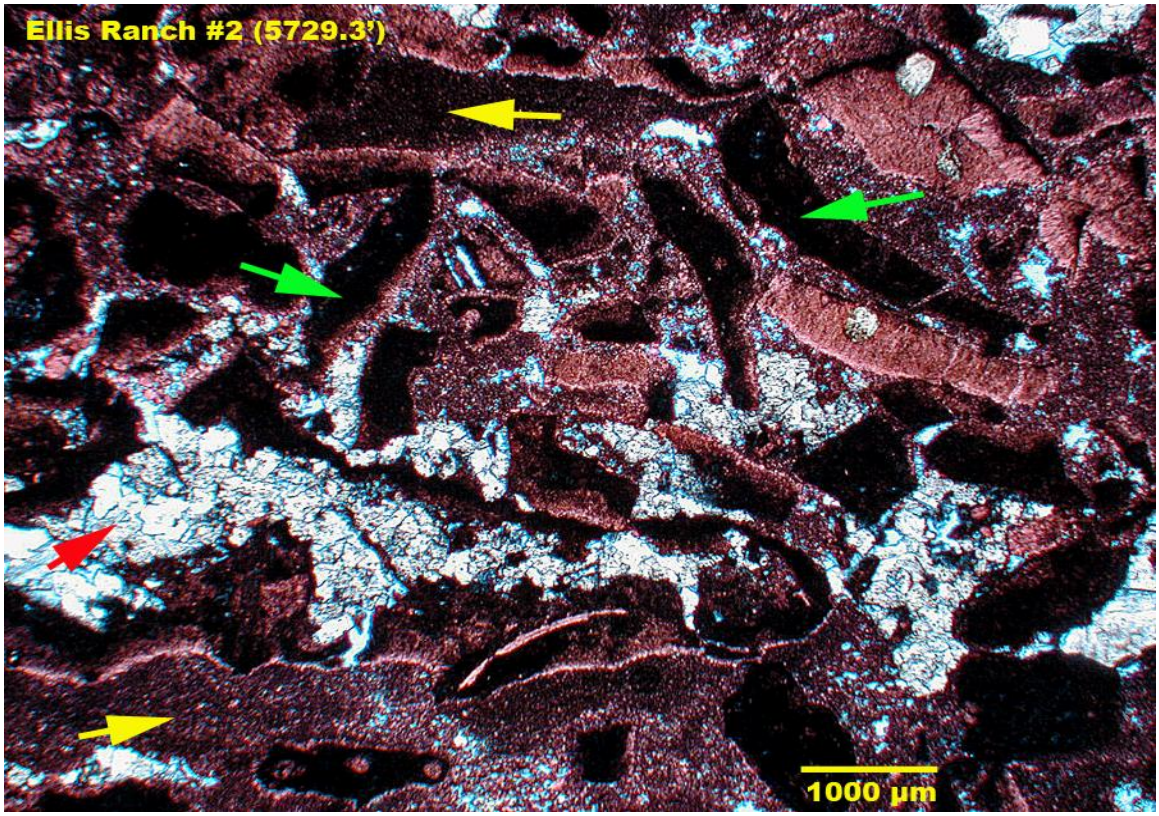

Figure 17. Thin section from 5729.3' viewed under plane-polarized light. Phylloid algae (green arrows) have a brecciated appearance from the collapse of algal framework caused by dissolution. Dolomite (red arrow) and micrite (yellow allow) form the matrix.

Core vs. Log Values

Ellis Ranch 2 core and log-derived values for effective porosity, bulk volume hydrocarbons, bulk volume water and permeability are displayed in Table 5, which is organized by depth and mound position: deeper subtidal, off mound debris, mound, and mound base. Average values were taken at each mound position. The absolute difference between core and log values was recorded and the average and standard deviation of the absolute difference is shown in Table 5. The one error found in the log-derived results is the result of a bad tool reading

from the density porosity log. The error is limited to the base of the mound and affects the effective porosity, bulk volume hydrocarbon, bulk volume water and permeability.

Table 5. Average core and log-derived values from different parts of the Rasberry Reef carbonate mound.

Environment	Depths, ft	PHIE, %		BVH, %		BVW, %		K, md	
		Log	Core	Log	Core	Log	Core	Log	Core
Deeper-Subtidal	5698-5703	5.87	6.98	1.57	2.2	4.3	4.77	0.14	5.64
Off-Mound Debris	5704-5715	4.74	4.5	1.05	1.35	4.16	3.16	0.2	1.12
Mound	5716-5735	8.02	9.45	2.12	3.39	6.12	6.07	0.49	72.17
Mound Base	5736-5737	0	1.69	0	0.48	0	1.21	0	0.03
Deeper-Subtidal	5738-5741	0.73	0.5	0	0.08	2.96	0.42	0	0.22
Average Difference		2.69		1.5		1.71		33.6563	
Standard Deviation Difference		1.91		1.22		1.1		94.8093	

The average difference between core and log-derived effective porosity is 2.69%. The standard deviation of the average difference is 1.91%. The log-derived values are just slightly out of the desired 2% range, but the log and core values still follow the same trends and the log-derived effective porosity can be used to identify mound reservoirs (Figure 18).

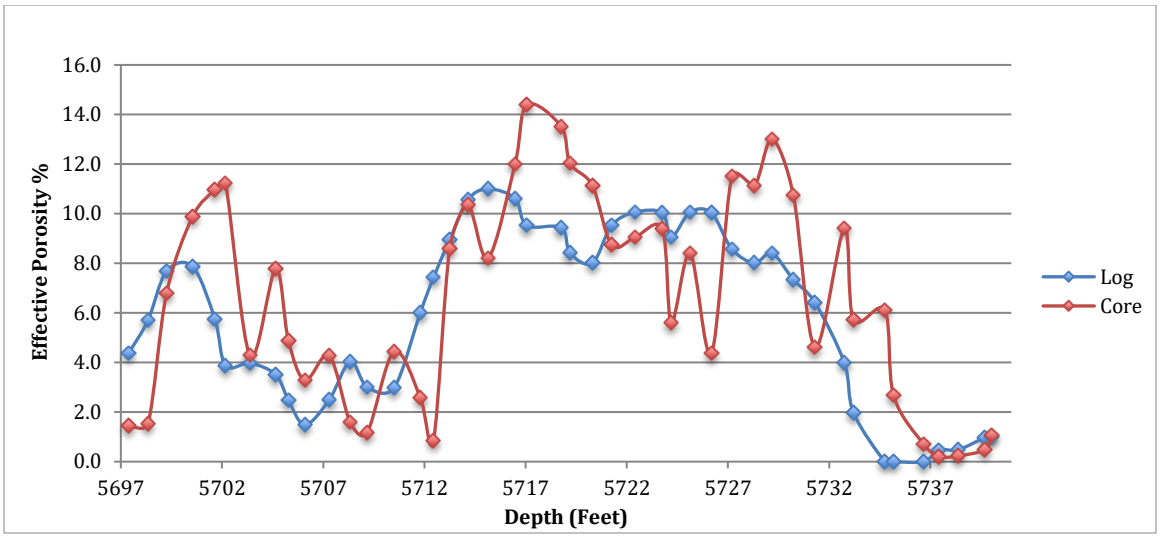

Figure 18. Log vs. Core Derived Effective Porosity.

The average difference between core and log-derived bulk volume hydrocarbons is 1.5%. The standard deviation of the average difference is 1.22%. Core and log-derived values follow the same trend (Figure 19). Log derived bulk volume hydrocarbons may be underestimated if the bulk volume water is overestimated.

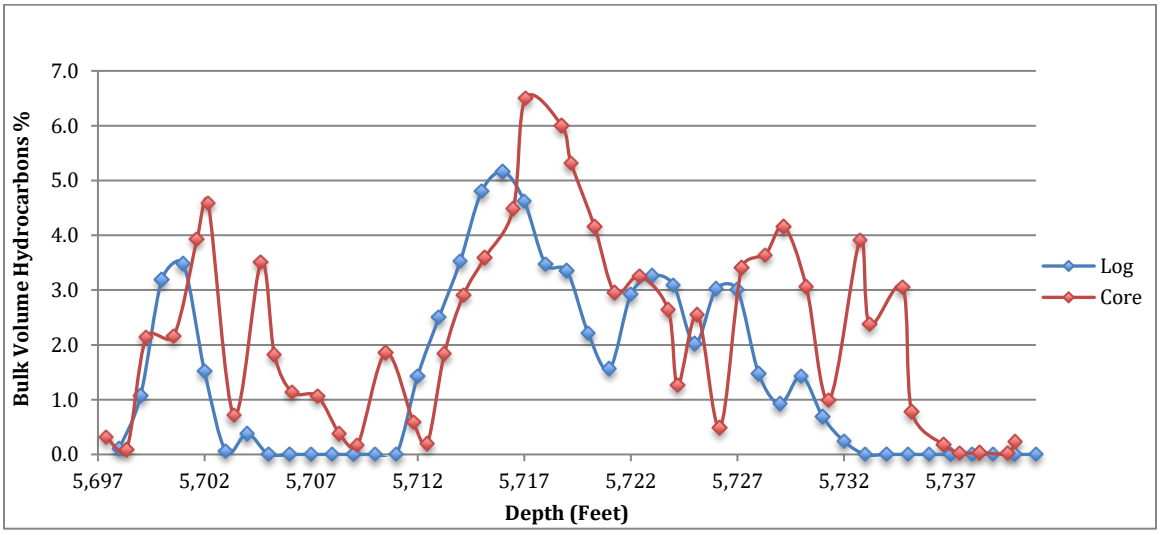

Figure 19. Log vs. Core Derived Bulk Volume Hydrocarbons

The average difference between core and log-derived bulk volume water is 1.71%. The standard deviation of the average difference is 1.1%. The trend for log-derived bulk volume water is slightly concerning. The log-derived values are not as sporadic relative to the core-derived values (Figure 20). In the upper mound reservoirs, log-derived bulk volume water is underestimated by 1-3%. Erratic bulk volume water core values are most likely the result of core handling subsequent to coring.

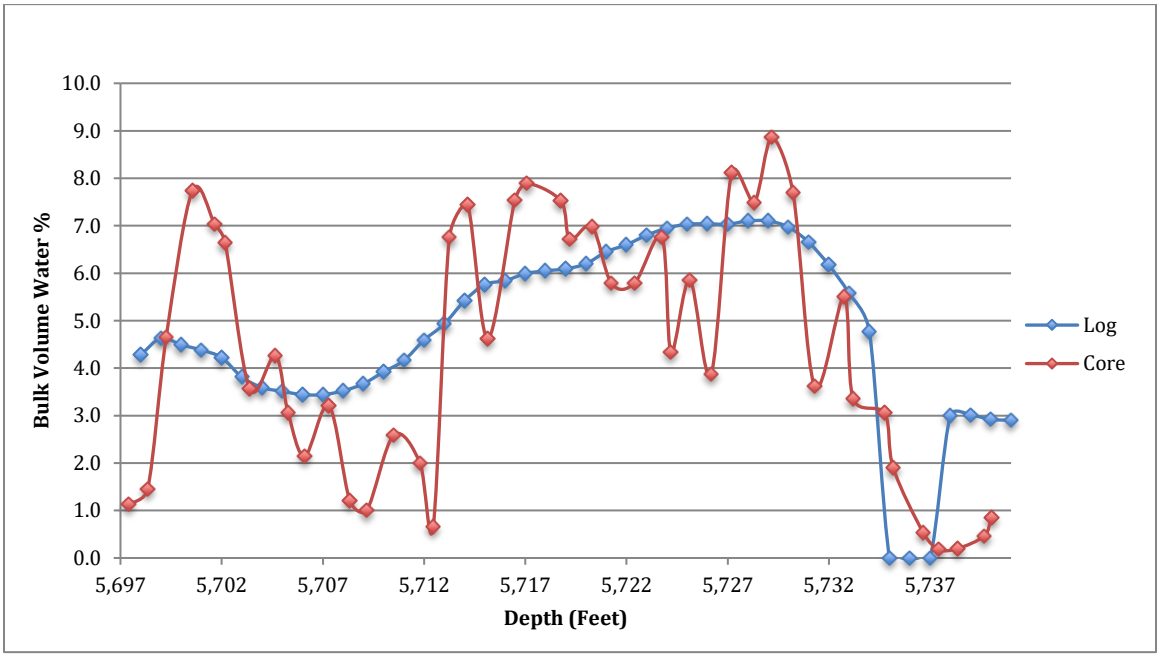

Figure 20. Log vs. Core Derived Bulk Volume Water.

The average difference between core and log-derived permeability is 33.7 md. The standard deviation of the average difference is 94.8 md. As noted in the methods, log-derived permeability is only valid for formations at irreducible water saturation. The large discrepancy in values is most likely due to the mound not being at irreducible water saturation. Log-derived values still follow the same

trend as core-derived values even though they may be off by one to two degrees of magnitude (Figure 21).

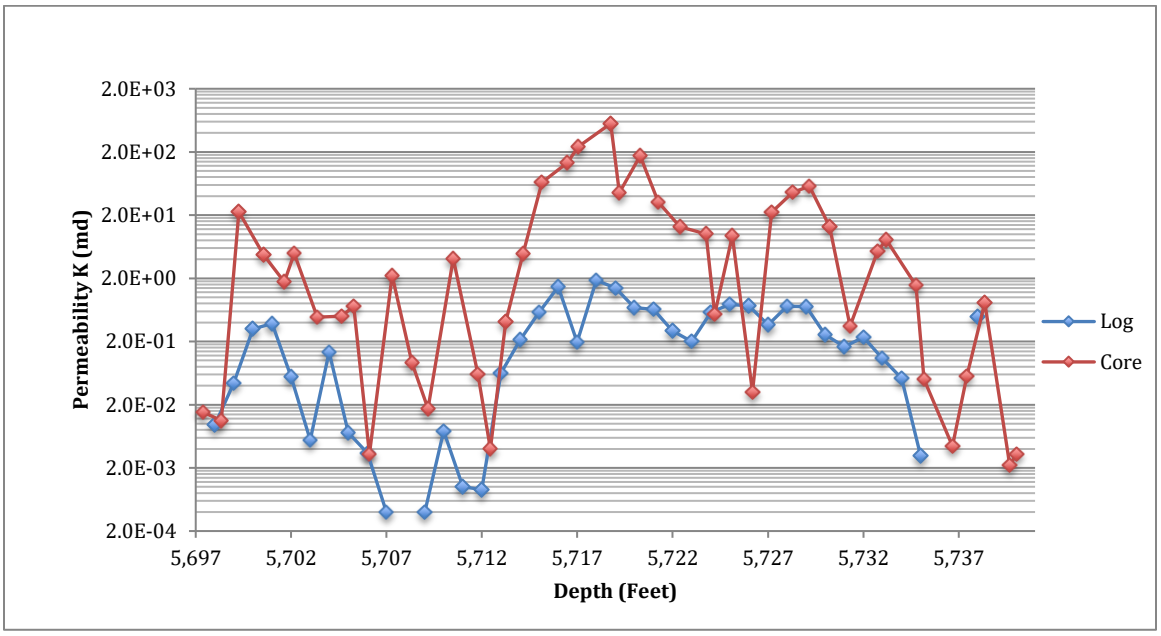

Figure 21. Log vs. Core Derived Permeability.

Petra Results

The Rasberry Reef neutron-density crossplot for all nine wells indicates a porous limestone with secondary amounts of dolomite (Figure 22). Porosity is approximately 5-15% with Ellis Ranch 7 recording the highest porosities (blue points). Ellis Ranch 3 (maroon points) and PFER 1 (red points) have the highest dolomite content. The Rasberry Reef top for PFER 1 is at 5710'. The off mound location and deep burial may have exposed the well to a higher degree of burial diagenesis hence the higher dolomite content.

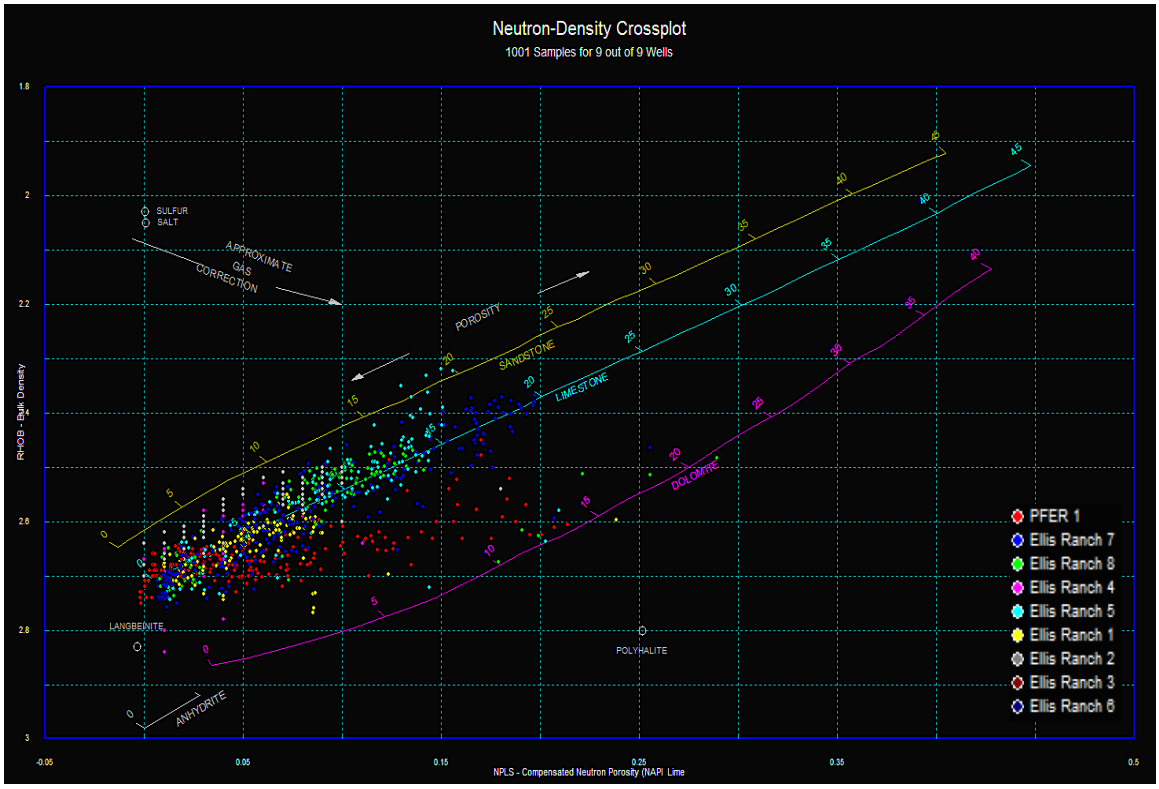

Figure 22. Rasberry Reef Neutron-Density Crossplot

The matrix identification plot for the Rasberry Reef indicates a limestone composed of almost 100% calcite (Figure 23). Ellis Ranch 3 has the most complex composition. The cluster of points has a composition of 10% dolomite, 20-40% quartz and 50-65% calcite. Dolomite contents are as high as 80% for some wells.

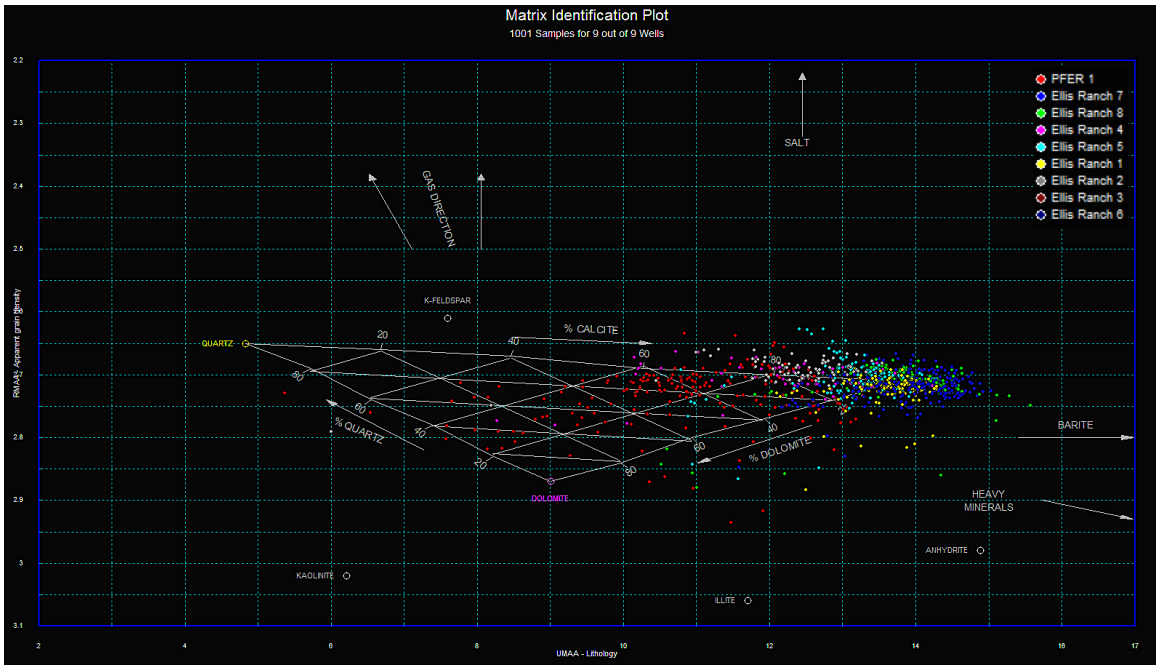

Figure 23. Rasberry Reef Matrix Identification Plot

The Buckles plot for the Rasberry Reef shows a reservoir not at irreducible water saturation due to the points not plotting on the same hyperbolic curve (Figure 24. Bulk volume water ranges from 4-12% with the majority of points falling on the 6% bulk volume water line. This is in line with the log-derived and core-derived values from Figure 20. A histogram of the water saturation is listed on the y-axis. The water saturation has a bimodal distribution with two peaks at 77% and 92%.

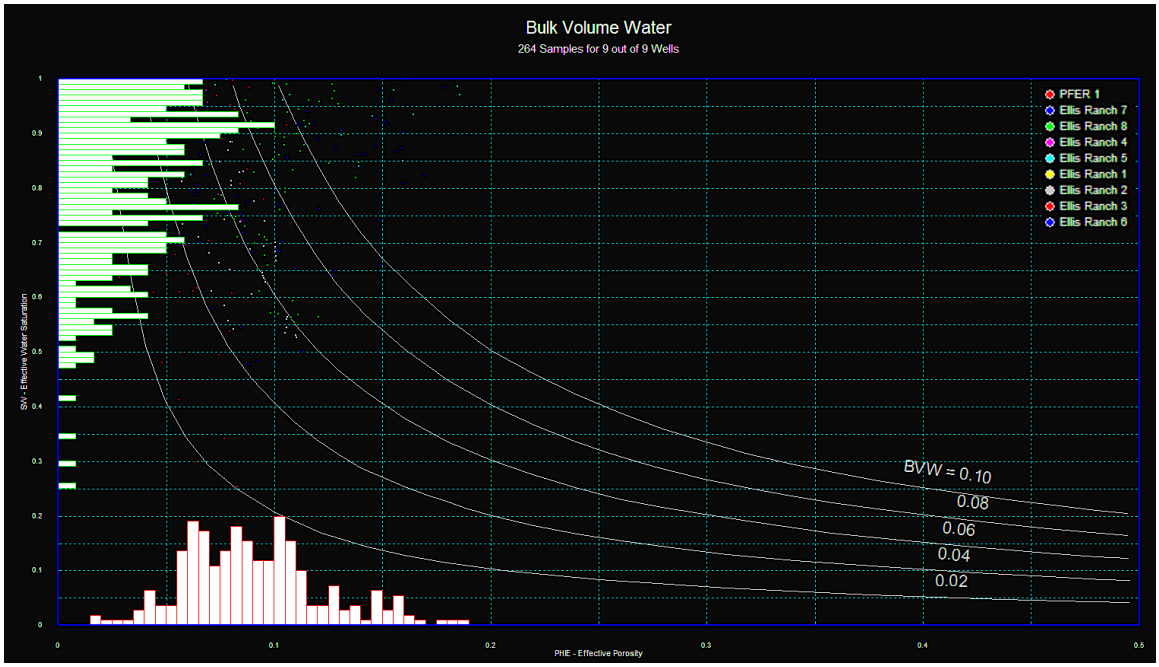

Figure 24. Rasberry Reef Bulk Volume Water

Log-derived effective porosity and permeability have a logarithmic relationship (Figure 25). Core-derived effective porosity and permeability is tied to mound position (Figure 26). The bafflestone mound and off-mound debris represent two potential reservoirs. The bafflestone mound has the best reservoir qualities with porosities from 8-15% and permeabilities from 10-500 md. The off-mound debris has porosities from 1-10% and permeabilities from 0-5 md. The lower permeability in the off-mound debris is tied to higher degrees of calcite cementation.

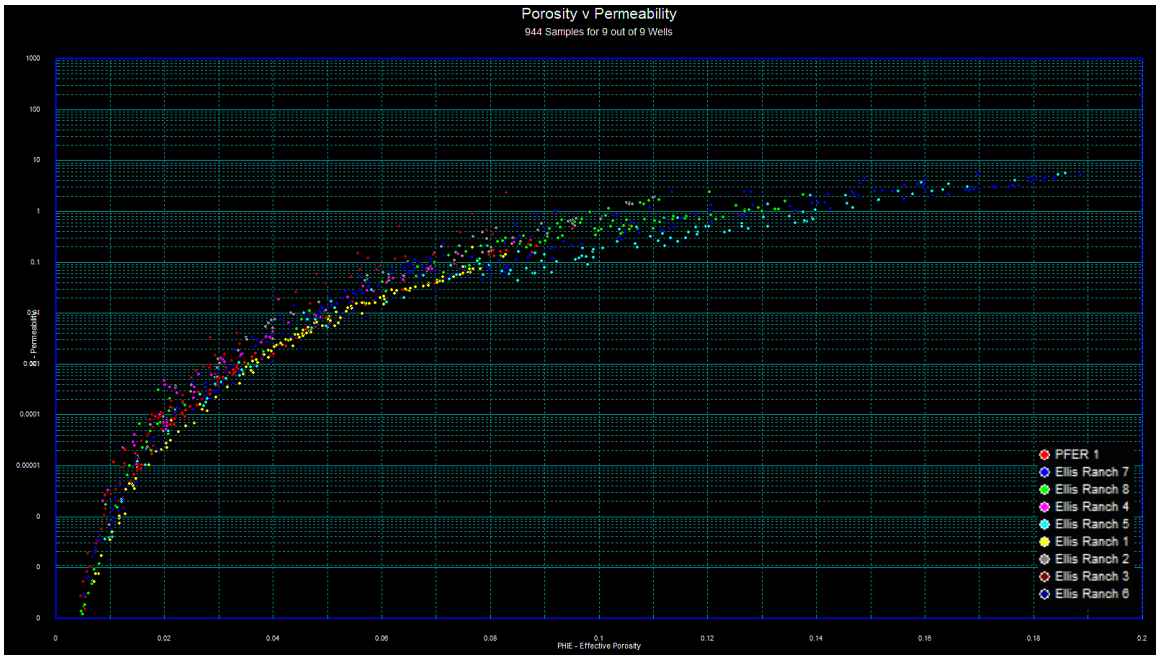

Figure 25. Log-derived Effective Porosity vs. Permeability

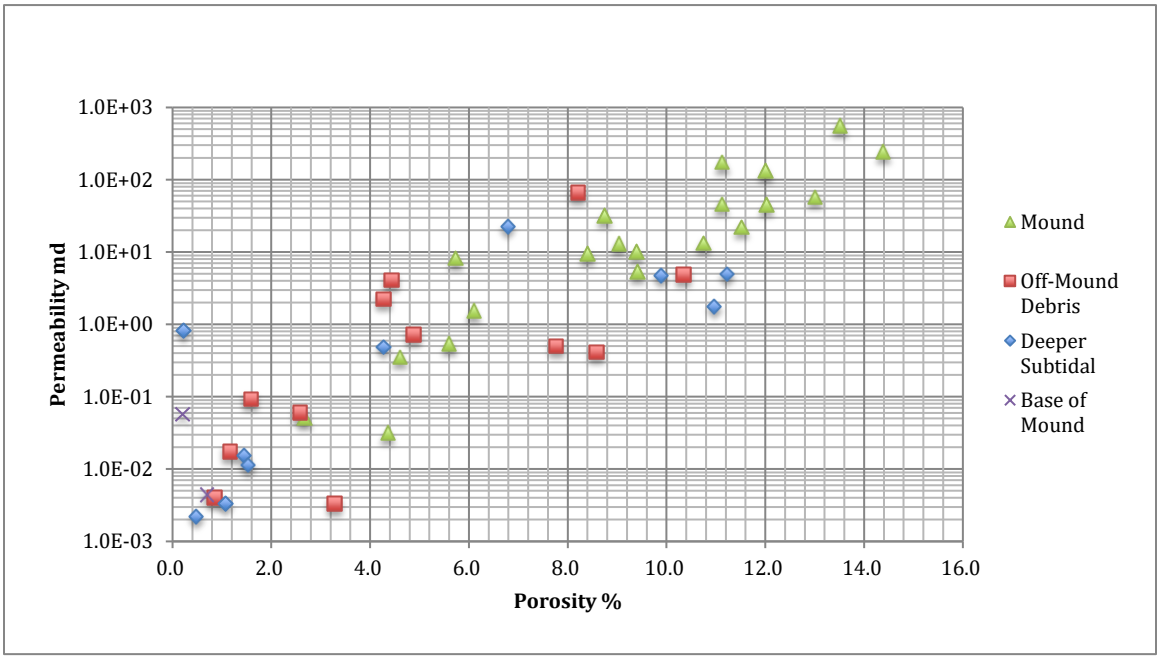

Figure 26. Core-derived effective porosity vs. permeability based off carbonate mound position

Chapter 6: Discussion

Petrophysical Evaluation

Identification of mounding cycles and parasequences occurs prior to reservoir evaluation. Mounding cycles are identifiable using the spontaneous potential and gamma ray logs. The spontaneous potential log can be used to identify the boundaries of permeable beds as well hydrocarbons. Spontaneous potential deflection is reduced in hydrocarbon bearing zones because of a phenomenon called hydrocarbon suppression (Asquith and Krygowski, 2004).

The beginning of a mounding cycle has a negative spontaneous potential deflection of 50-100 millivolts. Two mounding cycles or reef buildups are present for Ellis Ranch 2. The first cycle starts at 5772’ and the second cycle starts at 5740’ as indicated by the spontaneous potential log (Figure 27). Two mounding cycles are present for all wells except Ellis Ranch 7, Ellis Ranch 8 and PFER 1. The probable cause for this is their distal location relative to the mound complex. Ellis Ranch wells 7 and 8 have one identifiable mounding cycle in well logs that was part of the second mounding cycle. The Caddo-Strawn sequence boundary is marked by a gamma ray spike greater than 100 units. It is clearly marked for all nine wells.

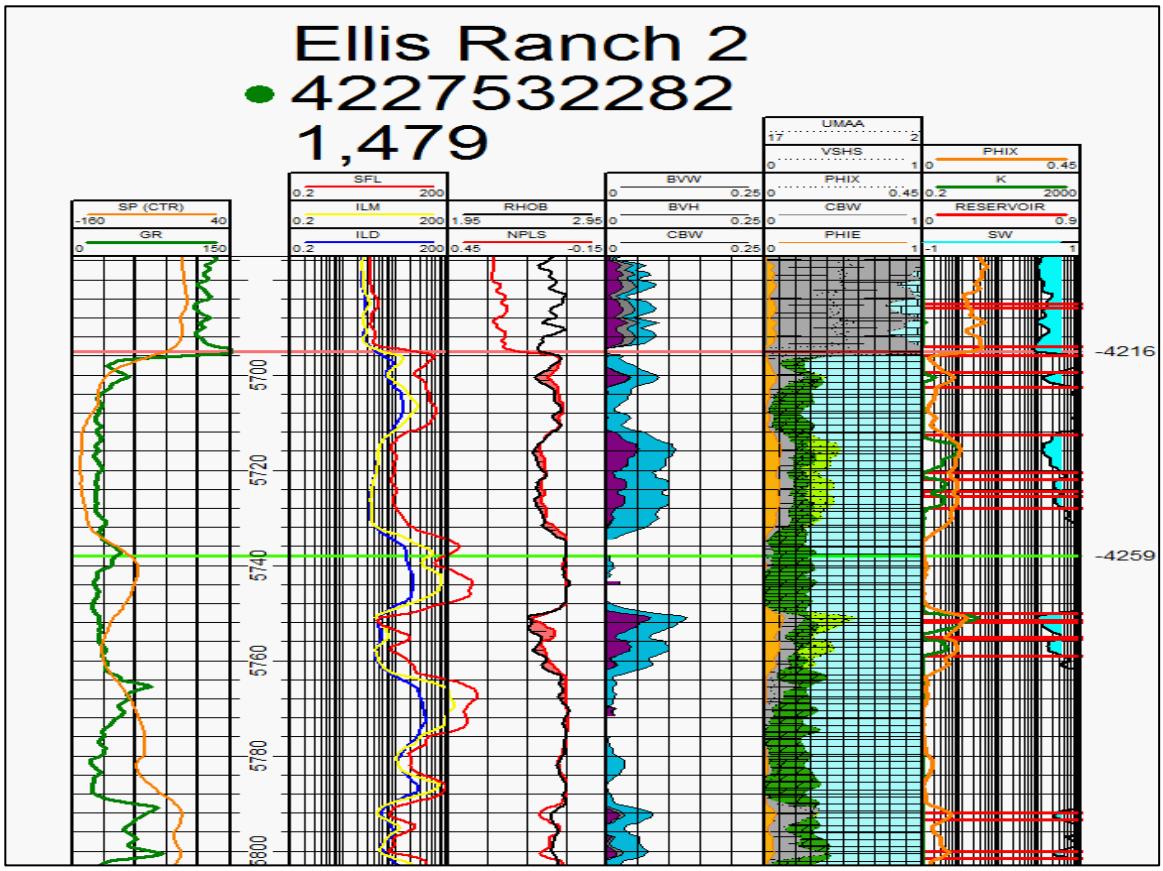

Figure 27. Ellis Ranch 2 log from 5675’ to 5800’.

Three reservoirs with potentially 40’ of pay are present for Ellis Ranch 2 (Figure 28). Pay flags were made with water saturations less than 75% and deep resistivity log readings greater than 10 ohm-ms. Pay flags are found in track 6. Water saturation with shading for saturations less 75% are found in track 6. Track 4 represents the total porosity of the rock-fluid matrix as the summation of the clay bound water, bulk volume water and bulk volume hydrocarbons. The total porosity ranges from 8-12% for all three reservoirs. Bulk volume hydrocarbons ranges from 3-6% for all three reservoirs. Neutron-density crossover is present in all three pay zones.

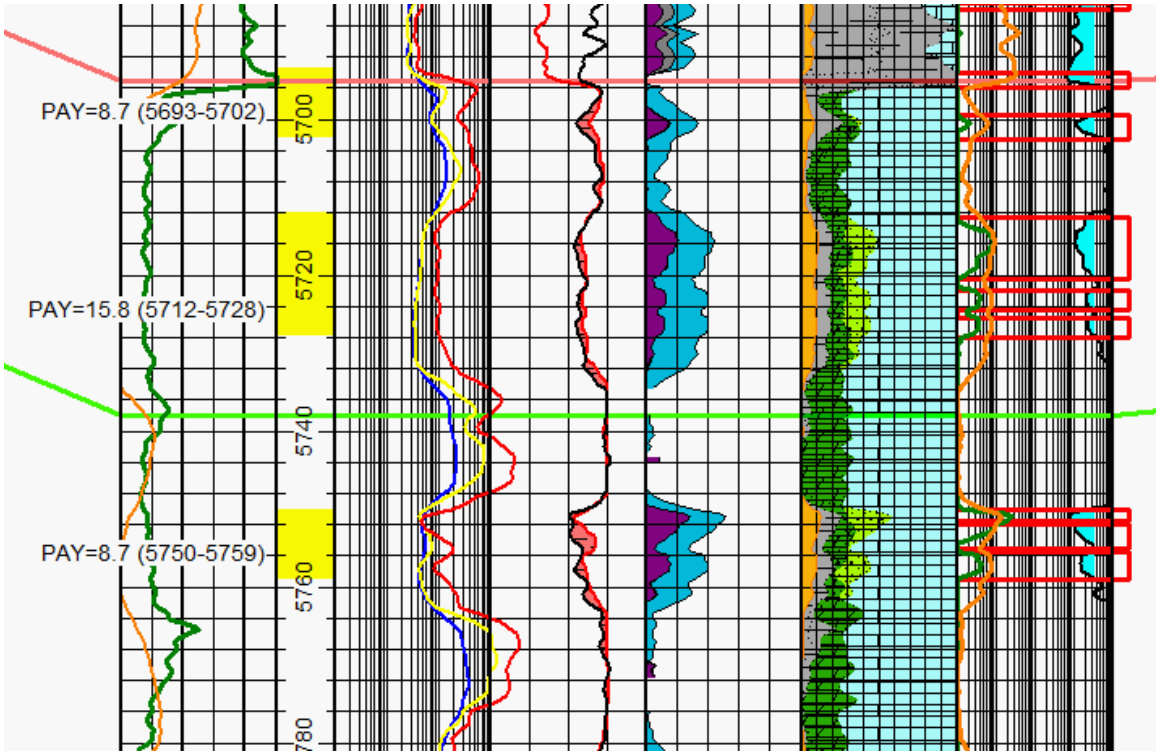

Figure 28. Ellis Ranch 2 pay zones.

Pay zones were picked for Ellis Ranch wells 1, 3, and 4 based on bulk volume hydrocarbons and observed resistivities (Table 6). The three wells were picked because of their proximal location to the Rasberry Reef mound crest and current production.

Ellis Ranch 4 has the best sustained resistivity for the Rasberry Reef and Caddo intervals (Figure 29). Resistivities greater than 20 ohmms are sustained over an 80’ section. Reservoir development would be difficult here because of low effective porosity. Effective porosity reaches 7-8% in the 5700’ and 5743’ reservoir but porosity is rarely greater than 5% over the entire section. The 5743’ reservoir had several pay flags. Acidizing and perforating the 5700’ to 5730’ section may help stimulate the production of the reservoirs.

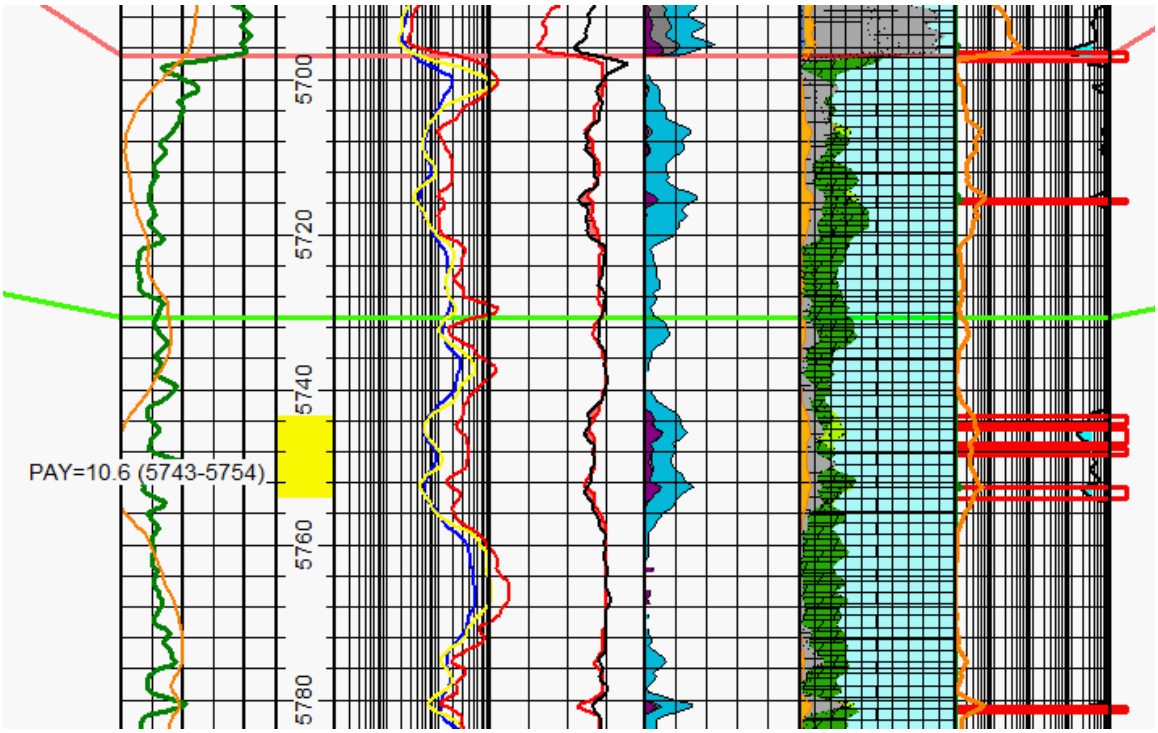

Figure 29. Ellis Ranch 4 log

The Ellis Ranch 3 Rasberry Reef section has some of the best petrophysical qualities from a reservoir development point of view (Figure 30). Three pay flags hit over the 20' section from 5660-5680'. Spontaneous potential did not deflect until after the 5680' mark. This could be an example of hydrocarbon suppression. There is a minimal deflection from the shale baseline so it could also be due to the shale content in the upper part of the reef. This is the only reservoir where bulk volume hydrocarbon is greater than bulk volume water. Bulk volume hydrocarbons ranges from 2-6% and bulk volume water ranges from 1-3%. There are good permeability spikes in the section as well. Resisitivity hovers around 20 ohmms. The Caddo Reef found at 5717' has good porosity and permeability but the high bulk volume water content makes it an uneconomical prospect.

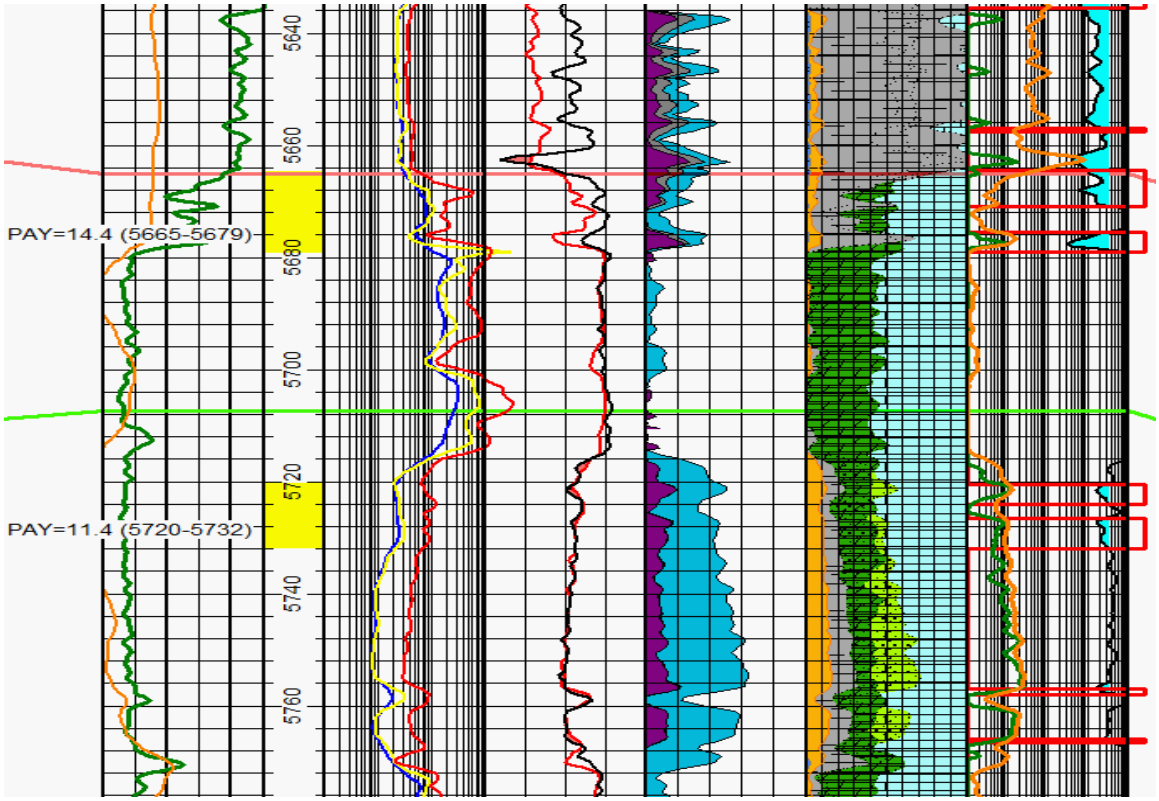

Figure 30. Ellis Ranch 3 log

Ellis Ranch 1 has produced 127,490 barrels of oil since it started producing on October 1, 2012 (Figure 32). The reservoir was perforated from 5673' to 5691'. There are no hydrocarbon indicators over this section, but there is good sustained resistivity. Values of Rw, a, m, and n used to calculate the Archie water saturation are the most likely cause of the lack of hydrocarbon indicators over the section. A water resistivity of 0.035 ohmm was used. If the resistivity of water was actually lower here, the water saturation would be lower and the bulk volume hydrocarbons would be higher. In addition to using constant values, low porosity makes it difficult to calculate the actual bulk volume hydrocarbons because it does not take into affect trapped hydrocarbons. Lower porosity and

high resistivity should not be overlooked because of this. The highest resistivity is found at 5720’ (Figure 31). This may merit exploration.

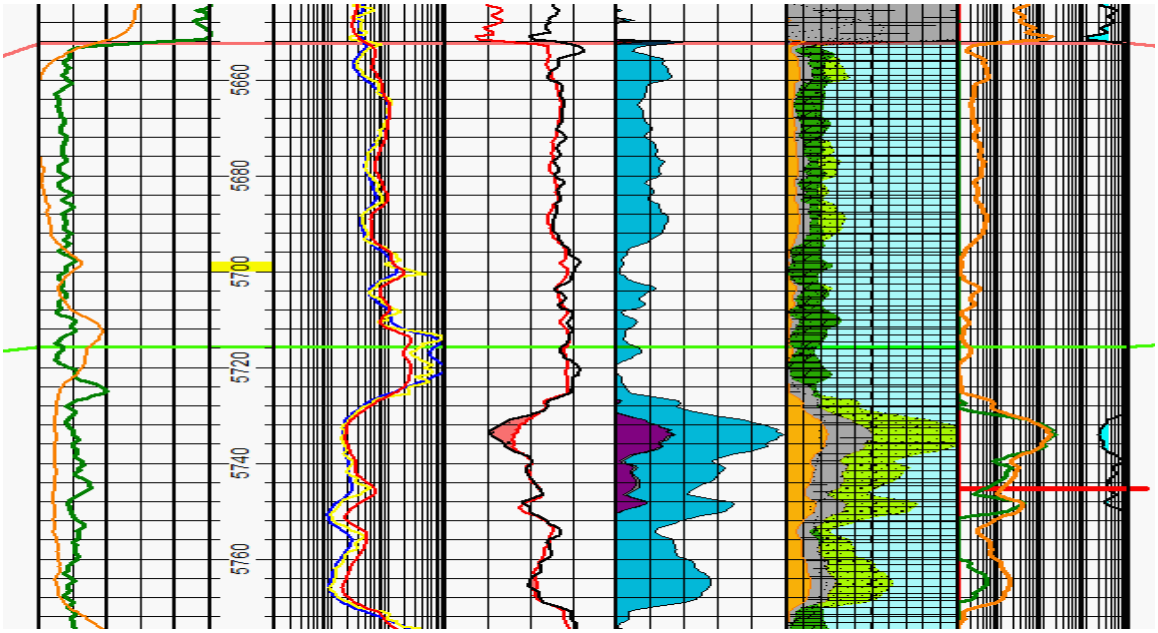

Figure 31. Ellis Ranch 1 log

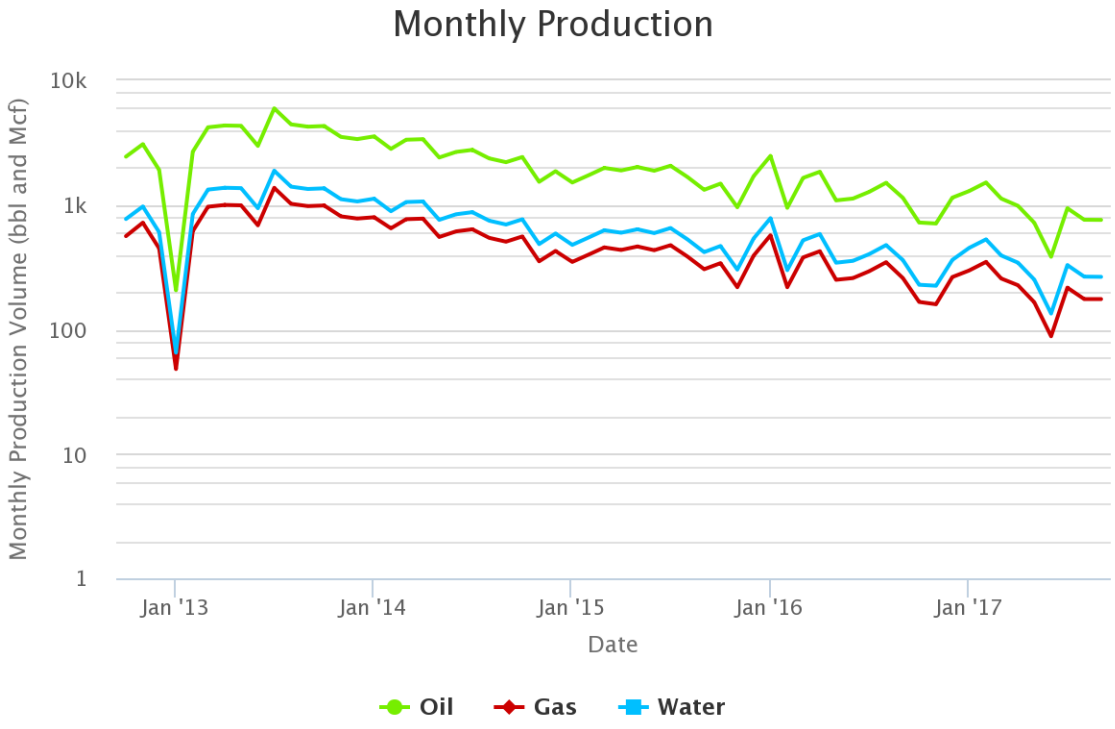

Figure 32. Ellis Ranch 1 Production

Table 6. Petrophysical properties for Ellis Ranch wells 1, 2, 3 and 4 Prospects

	Ellis Ranch 1		Ellis Ranch 2			Ellis Ranch 3		Ellis Ranch 4	
Depths	5673-5691	5728-5750	5696-5704	5712-5732	5750-5762	5660-5680	5717-5768	5700-5720	5743-5754
Pay Height	18'	32'	8'	20'	12'	20'	51'	20'	11'
SP Deflection	100	80	>120	>120	100	20	80	90	100
Resistivity	4-40	2-8	20-200	4-20	5-20	4-200	2-20	4-200	5-50
Neutron-Density Crossover	No	Yes	Yes	Yes	Yes	No	No	Yes	Yes
Borehole Invasion	No	No	Yes	Yes	Yes	Yes	Yes	Yes	Yes
Effective Porosity	4-7%	10-25%	3-8%	3-11%	4-12%	3-12%	5-16%	2-8%	3-7%
BVH	0%	3-7%	4%	3-5%	4-6%	2-6%	2-5%	0-1%	1-3%
BVW	4-7%	8-18%	2-4%	3-8%	4-7%	1-3%	5-13%	2-8%	2-5%
Formation	Rasberry	Caddo	Rasberry	Rasberry	Caddo	Rasberry	Caddo	Rasberry	Caddo

Seismic Analysis

Depositional Model

Seismic analysis provided insight into the depositional environment and structure of the prospects. The Rasberry Reef depositional environment is best described as a rimmed platform with shelf-edge reefs and an isolated barrier reef. In the northwest corner, there is a dip-oriented shelf-edge reef system with progradational to aggradational stacking (Figure 33). Deposition of the reef is wave controlled as noted by the strike orientation. The shelf-edge reef is a topographic buildup with internal bioherms and encrusting lime sand shoals. The phylloid algal bioherms experienced subaerial exposure prior to burial diagenesis and represent the best carbonate reservoirs. The phylloid algae have aragonitic compositions that are susceptible to dissolution during diagenesis. Phylloid algal bioherms were common during the Pennsylvanian as the global sea chemistry transitioned from calcite to araongite-dominated (Wright, 2011). The inner lagoonal area found landward or north of the shelf edge reef contains laminated

carbonate sand bodies and grainstones that onlap the shelf edge. The sand bodies were transported from the Red River Uplift and Electra Arch.

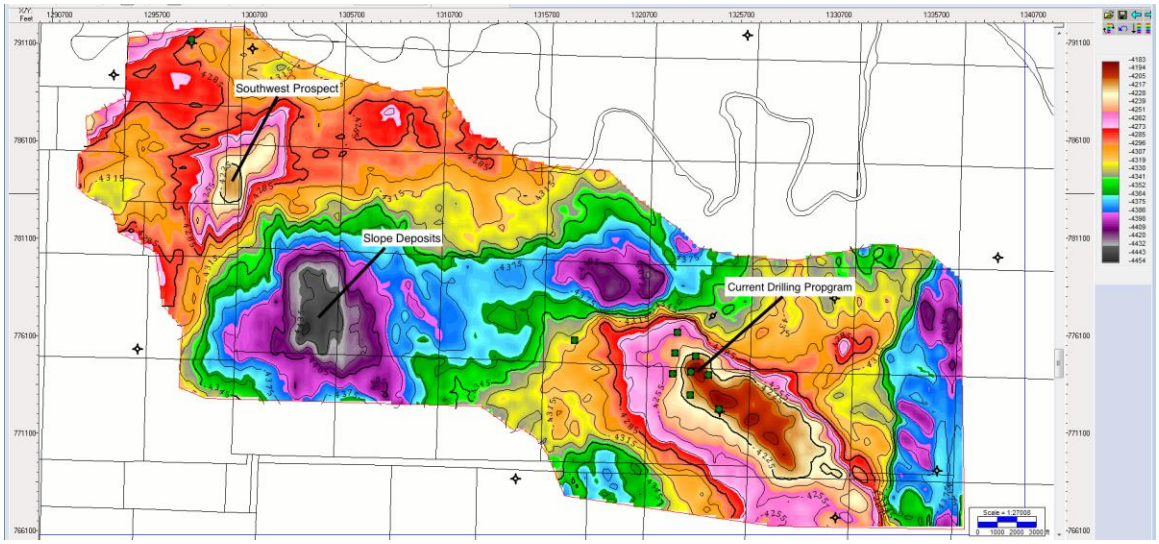

Figure 33. Rasberry Reef Depth Map

Moving from the northwest to the southeast there is a dropoff marked by an accretionary slope. Sediments were transported into this low area by slumping and debris flows. Three slope aprons are identifiable on the Rasberry Reef isopach map. Submarine fans can be found in the Strawn sequence when the Strawn siliciclastics prograded across the basin.

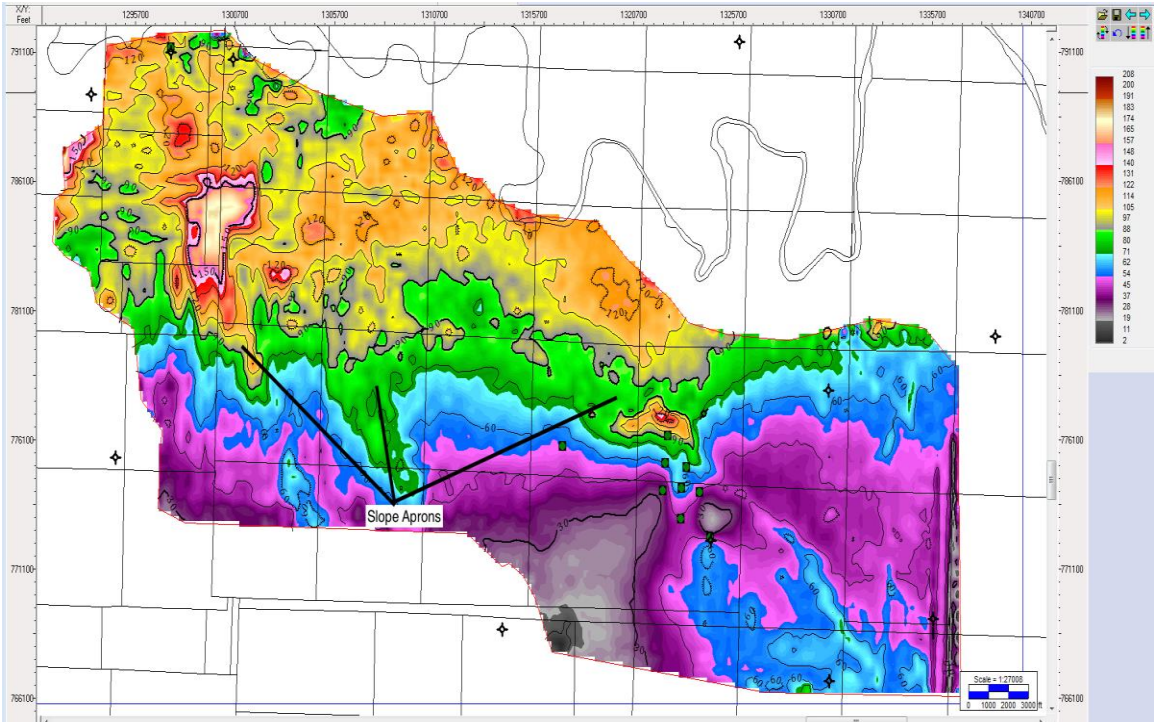

Figure 34. Rasberry Reef Isopach Map

In the southeast part of the map we have the current drilling program focused on an isolated carbonate platform with internal phylloid algal bioherms and capping mud mounds (Figure 33). The phylloid algal bioherms are the primary reservoir facies of the drilling program. The carbonate platform is debatable as to if it is a barrier reef, pinnacle reef or patch reef. The reef extends for over 15,000’ from the northwest to the southeast and is 5,000’ across. Four carbonate mounds are identifiable on the depth map with each representing a potential reservoir.

Stacking Patterns

Sedimentation rates kept up with subsidence rates during deposition of the Pennsylvanian carbonates. This is not surprising since carbonate sedimentation rates exceed subsidence rates and sea level fluctuations (Boggs,

2012). The northwest and southeast carbonate buildups have aggradational stacking patterns. The lowstand channel deposits onlap and toplap these carbonate buildups (Figure 36). Reef sag is apparent from the Caddo Reef top to the Caddo Reef base in the southeast. This time period represents the main reef-building phase.

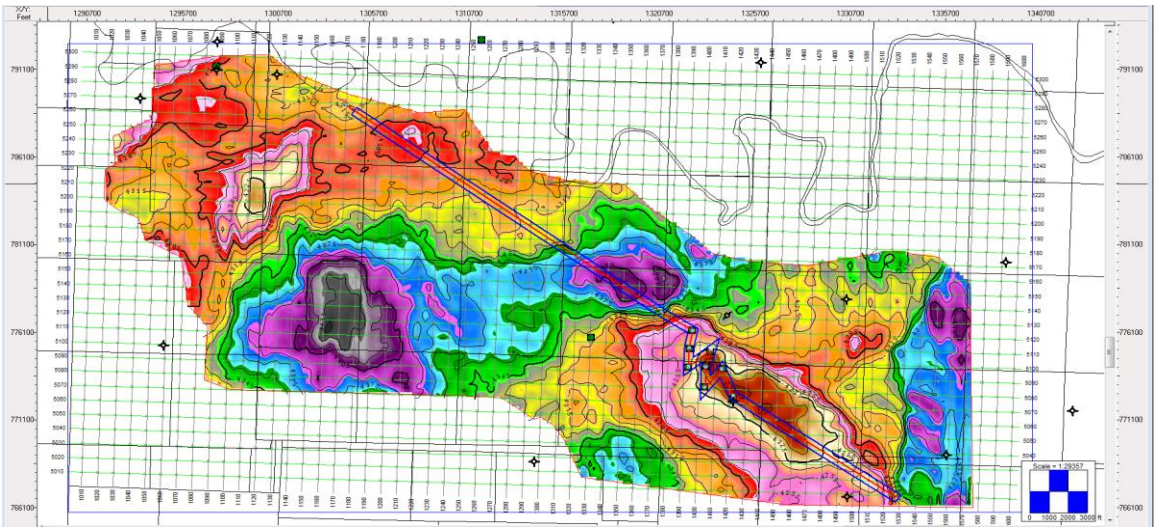

Figure 35. Arbitrary Line across shelf margin, lowstand deposits and isolated reef.

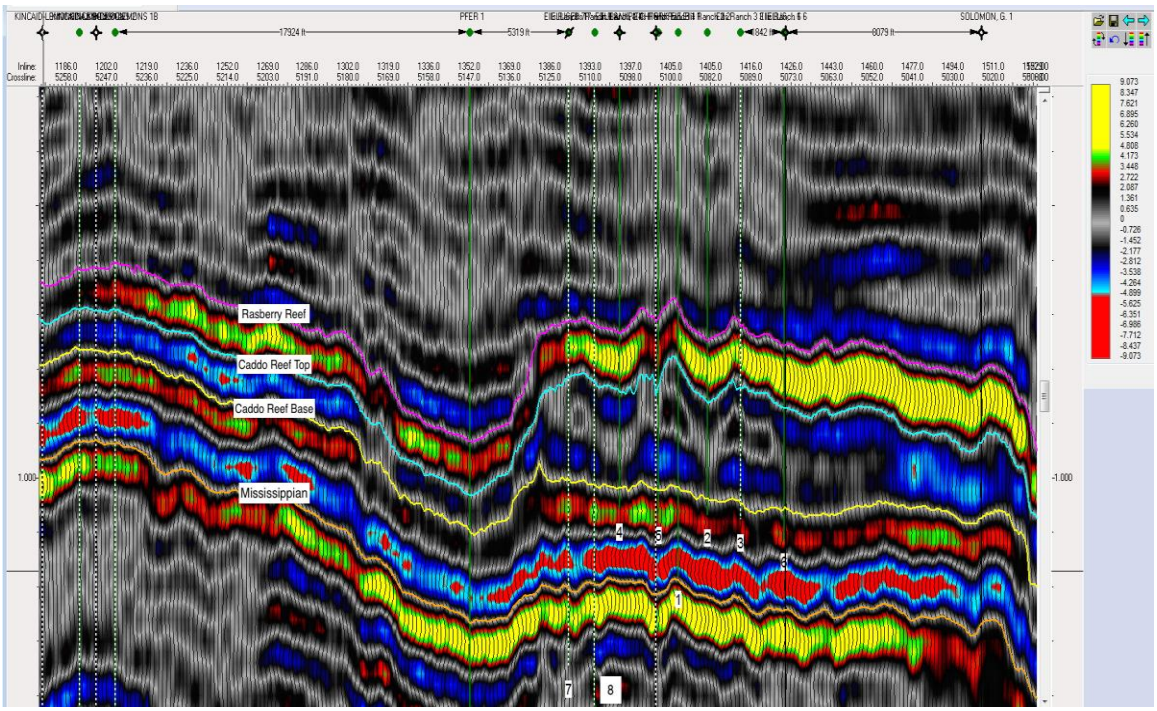

Figure 36. Arbitrary line cross-section view (amplitude)

As noted with the Paradox Basin and Big Lime mounds, the Rasberry Reef mounds have a structural trend in the northwest-southeast direction (Figure 37). The *string of pearls* term is commonly used when describing the trend of these mounds. Each mound in the string of pearls represents a potential reservoir. The reservoirs are clearly identifiable in cross section view with some degree of reef sag occurring in each locality (Figure 38). Drilling has focused on the off mound debris and mound talus of the first and second mounds.

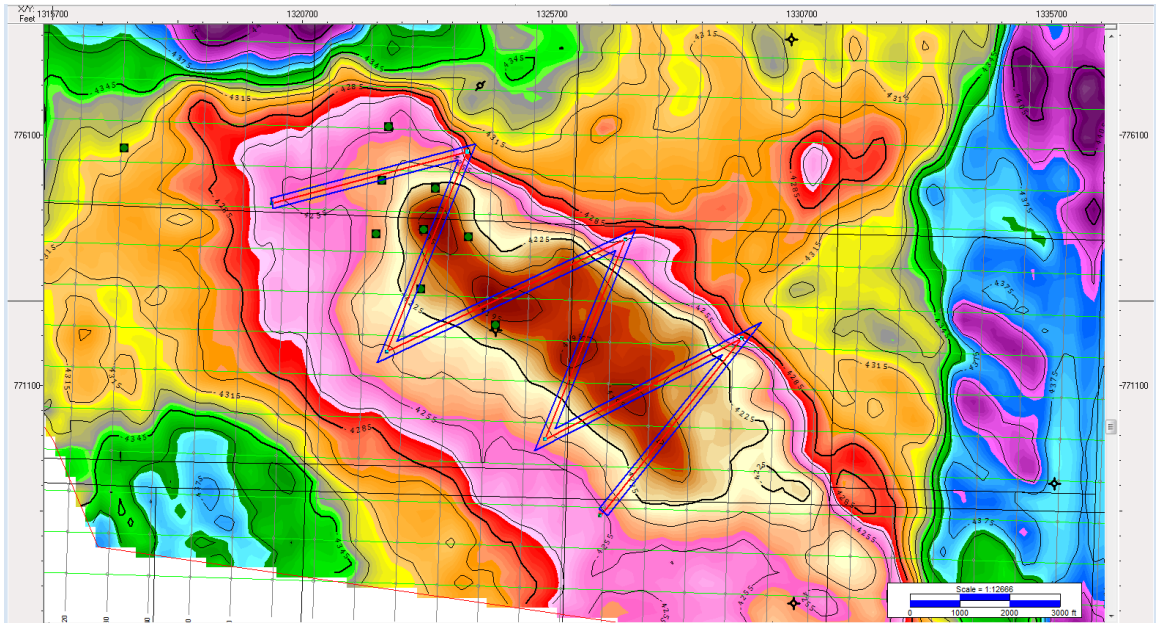

Figure 37. Arbitrary line across carbonate mounds.

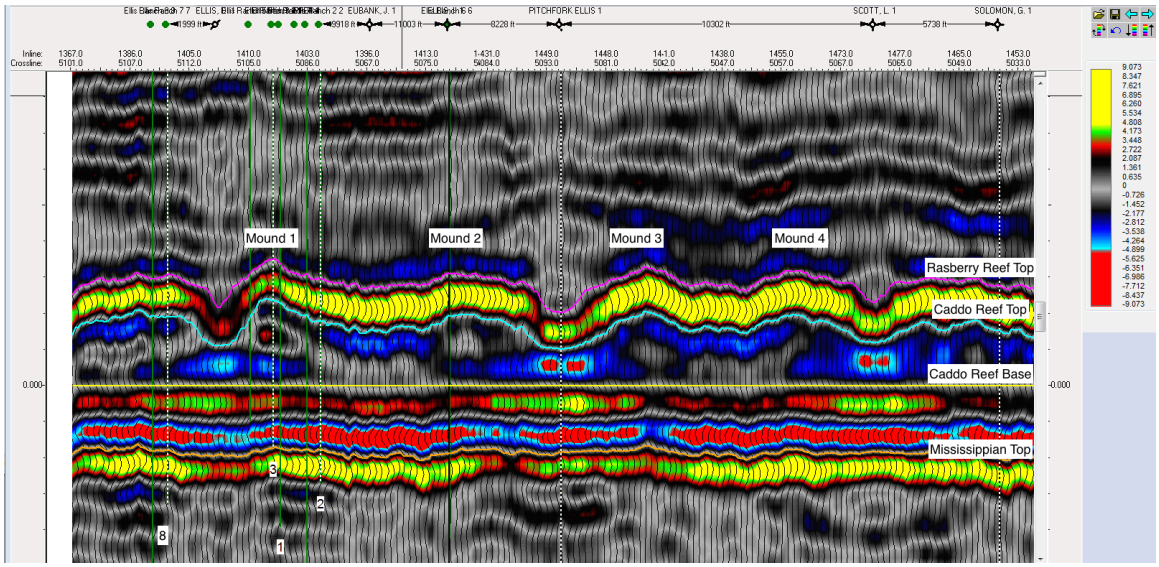

Figure 38. Flattened cross section view of mounds

Instantaneous Frequency Attribute

Seismic attributes are measurements derived from seismic data that highlight reservoir properties (Herron, 2011). Seismic amplitude is one of the most commonly used attributes when viewing seismic data. The instantaneous

frequency attribute is represented as the time derivative of the phase or the rate of change of the phase. It is used to identify lithology variations, fracture zones, the edges of low impedance beds and hydrocarbons. Fracture or porous zones have lower frequencies caused by hydrocarbon absorption effects (Sarhan, 2017). Time slices of the instantaneous frequency attribute can be used to map the drainage areas and extent of the reservoirs.

Instantaneous frequency correlates with a lithology variation, increase in porosity and hydrocarbons. There are three continuous low frequency beds through Ellis Ranch wells 6 and 2 (Figure 39). At the top of the first low frequency bed, 5520', there is a change is lithology from a shale dominated rock to a shale with significant volumes of limestone (Figure 40). Frequency ranges from 14 to 28 hz within the bed. At the top of the second low frequency bed, 5594', there is an approximately 3% increase in porosity. Bulk volume hydrocarbons increase from 2% to 4.5% within the bed. Frequency ranges from 0 to 15 hZ within the bed. The third low frequency bed is found in the Caddo Reef section and correlates with an increase in resistivity and change in lithology. Ellis Ranch 6 has almost zero porosity in the low frequency bed (Figure 41). The lithology changes from a sandy limestone to a dolomitic limestone at the low frequency contact. When the bed hits zero porosity, there is a spike and separation in the deep and medium resistivity logs. Deep and medium resistivity logs hit 200 ohms and have significant separation from the shallow resistivity log. The resistivity is sustained from 5800' to 5860'. The low frequency does not extend over that range, but it is a good indicator of the top of a resistive section and potential

hydrocarbon-bearing zone.

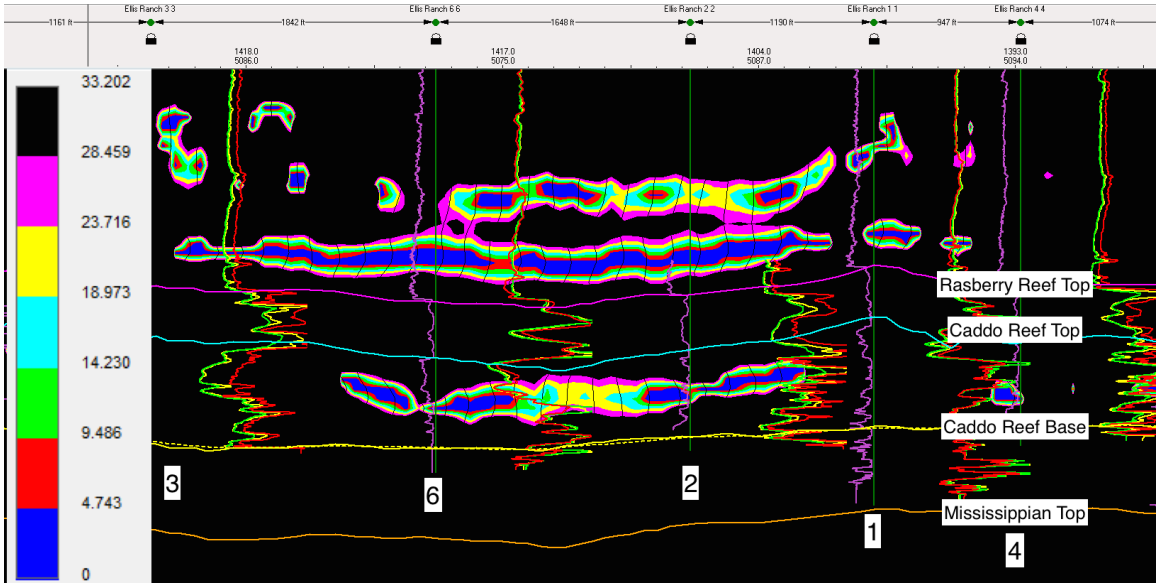

Figure 39. Instantaneous frequency attribute through Ellis Ranch wells 3-6-2-1-4 with neutron porosity and resistivity logs included.

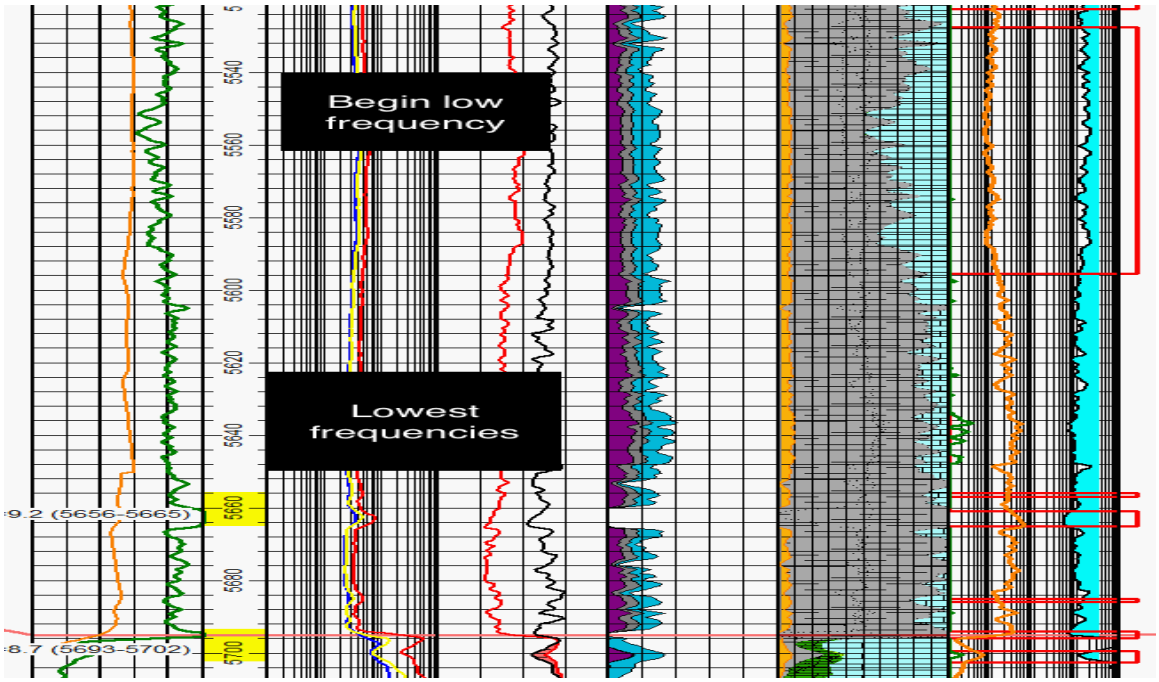

Figure 40. Ellis Ranch 2 well log 5520-5700’

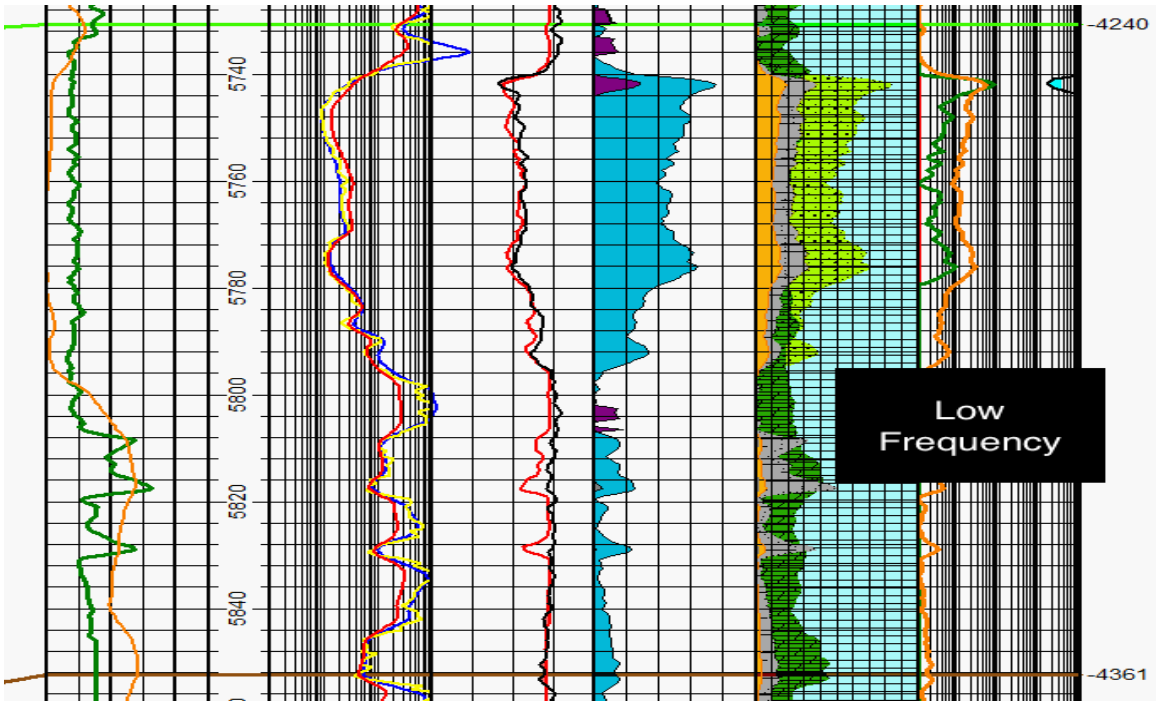

Figure 41. Ellis Ranch 6 well log-Caddo Reef

Instantaneous frequency timeslice mapping is used to identify widespread deposition and structures. Figures 42 to 46 show the deposition of a strike discontinuous channel fan complex in the southwest part of the map. Following deposition of the Rasberry Reef carbonate mounds, sea levels rose and the reef was drowned by mudstone deposition. Well logs and a black phosphatic shale at the top of the core section support this. The channel fan complex is identifiable when the instantaneous frequency attribute is applied. High porosity, hydrocarbon bearing channels have low frequencies less than 10 Hz that can be traced across the reef as the fan prograded through. As the fan prograded, it eroded away aragonitic grains from the shelf edge and deposited them on the foreslope and basin floor as channels and basin floor deposits. These deposits can form excellent hydrocarbon reservoirs if they have a good trap and seal.

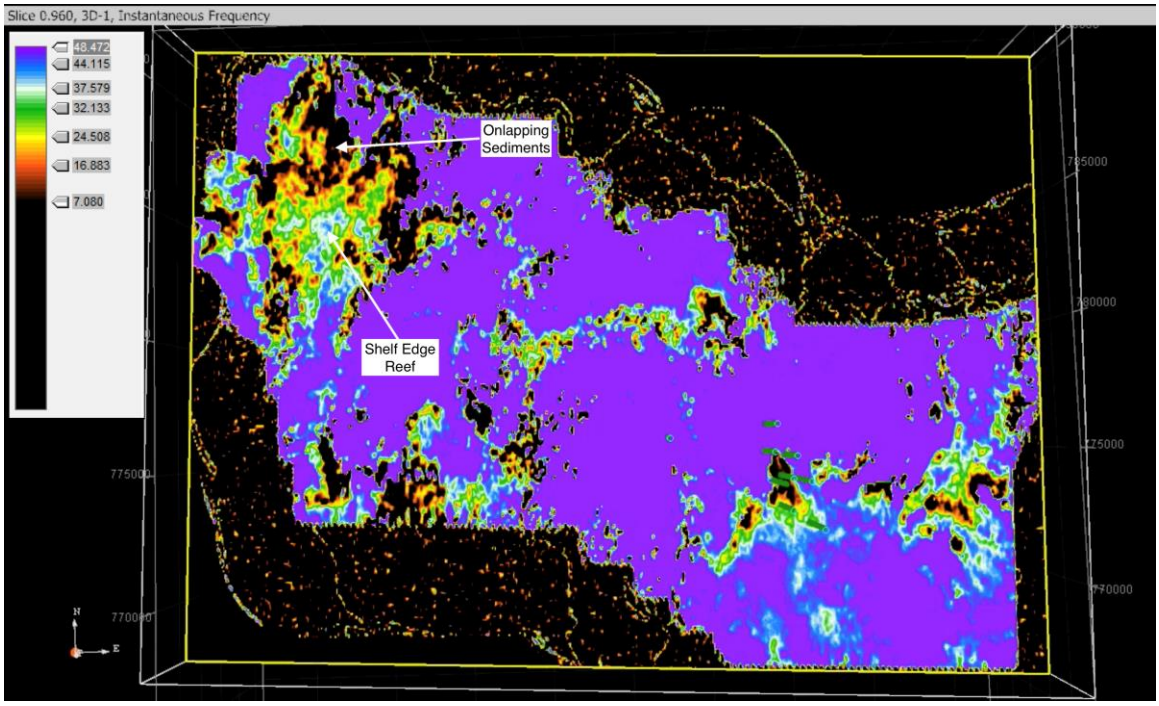

Figure 42. Timeslice 0.960-Instantaneous Frequency

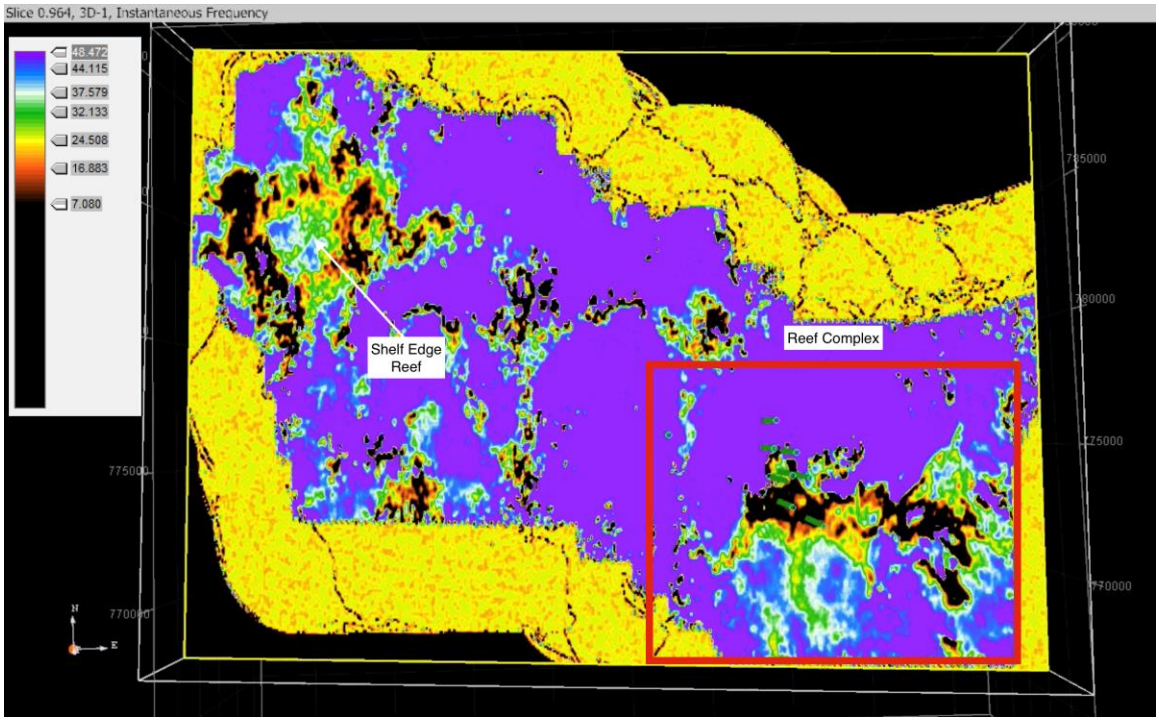

Figure 43. Timeslice 0.964-Instantaneous Frequency

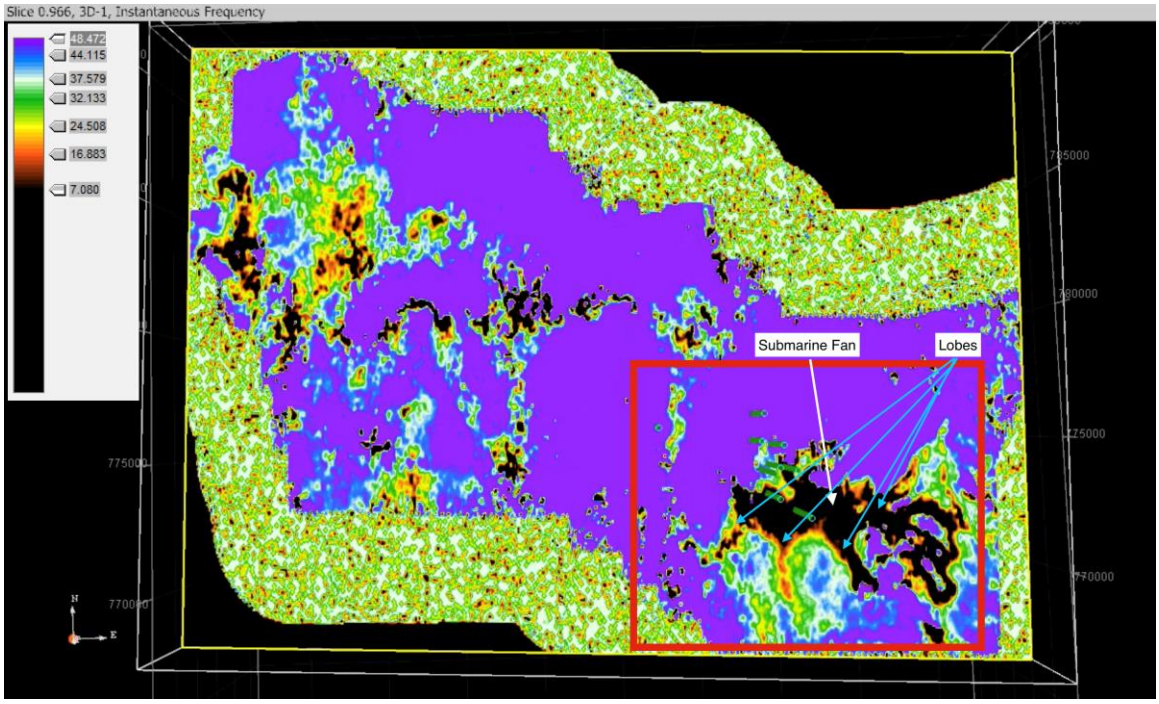

Figure 44. Timeslice 0.966-Instantaneous Frequency

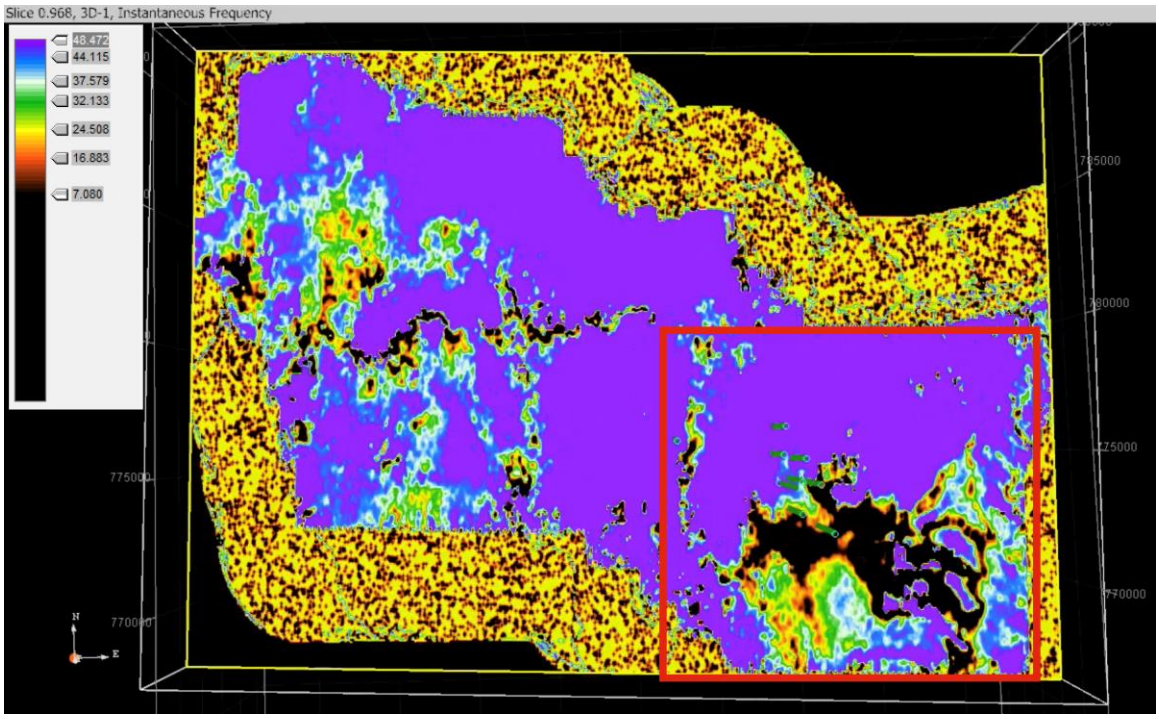

Figure 45. Timeslice 0.968-Instantaneous Frequency

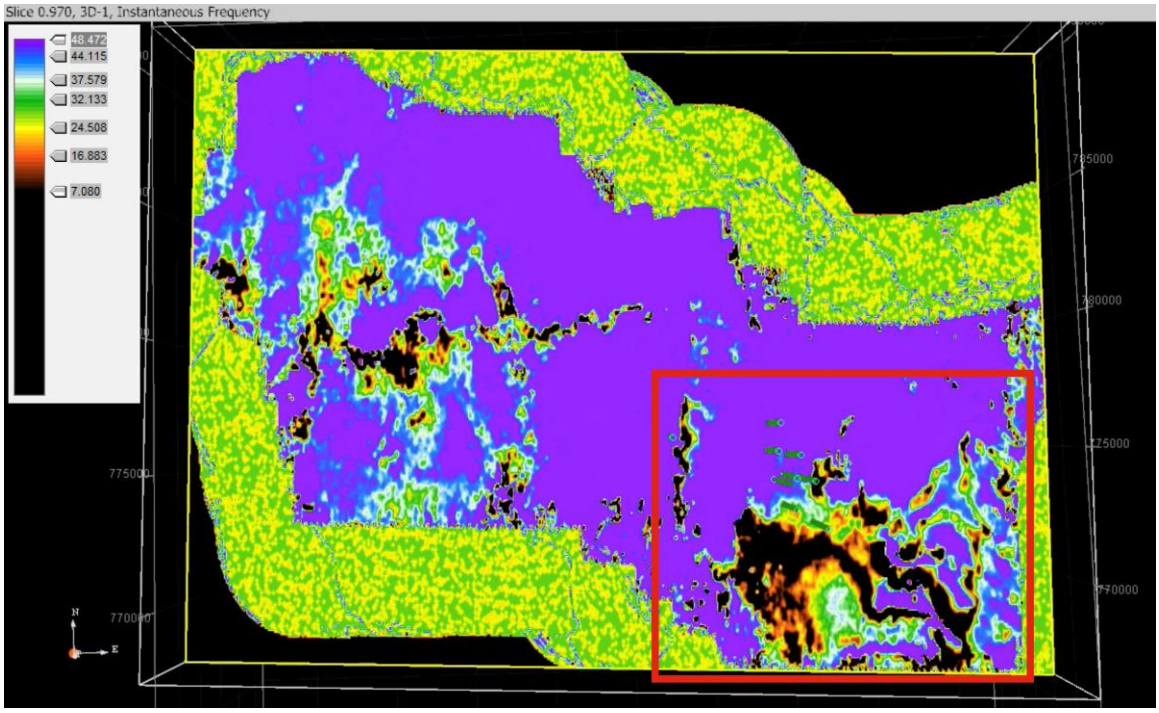

Figure 46. Timeslice 0.970-Instaneous Frequency

The structure of the foreslope plays a key role in trap formation. The foreslope has an escarpment margin with a draping accretionary margin deposited above (Figure 47). The onlapping sediments part of the escarpment margin are grain shedding and hemipelagic-dominated. Aragonitic phylloid algal grains are shed off the shelf edge and deposited on the margin with hemipelagic muds. The sediments are detached from the reef edge. This is necessary to form a trap against the foreslope. As the channel complex prograded across the reef, the reservoir was buried in low porosity mudstones and channel deposits. The channels are accentuated by their low frequencies. There are four potential stratigraphic traps for the reef and channel complex: reefal upper slope, toe-of-slope apron, channelized fans and basin floor fan. The reefal upper slope has already been proven as a hydrocarbon-bearing zone. The onlapping sediments

are part of the toe-of-slope apron. They represent the best potential reservoir. The closure against the foreslope combined with the untapped potential make it an attractive play. Channelized fans and basin floor fans are an attractive play as well, but well bore placement is key because of the limited lateral extent.

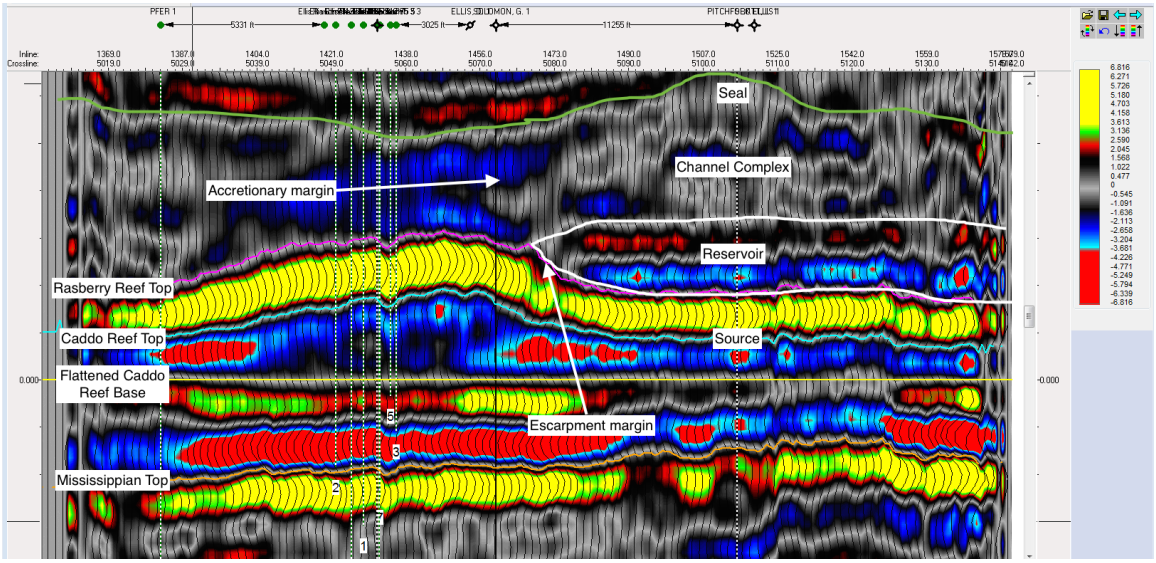

Figure 47. West-east cross section across reef

Instantaneous frequency is used to outline the structure of the Caddo Reef in Figure 48. The Caddo Reef has porosities ranging from 10-20% for Ellis Ranch wells 1, 3, 5, and 6. The porosity highlighted by the low frequencies can be traced across the reef in the northwest-southeast direction. This is in line with the structural trend of the reef. The instantaneous frequency also highlights the impedance and lithology contrasts between the reef and surrounding environment. The outline of the reef is highlighted by the high-low frequency contrast.

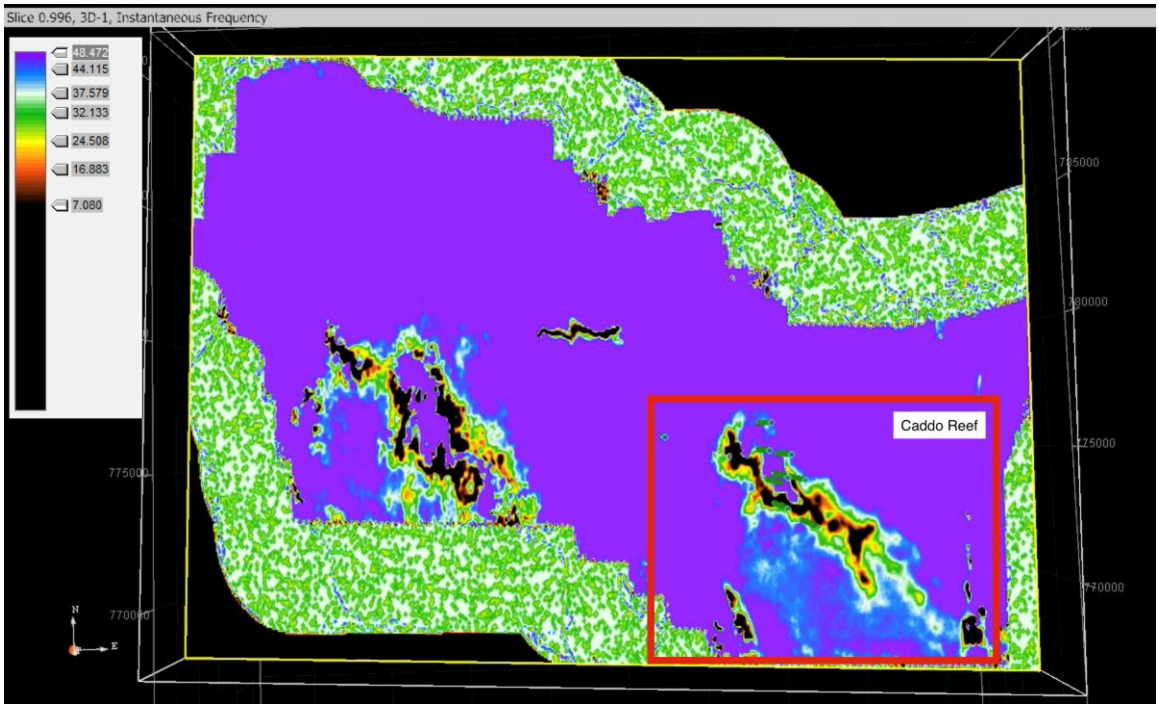

Figure 48. Timeslice 0.996-Instantaneous Frequency

Prospect Evaluation

The northwest shelf edge reef has all the characteristics of a viable hydrocarbon reservoir. It has low frequency attenuations indicating good porosity and widespread extent totaling 1,983 acres (Figure 49). The extent of the reservoir is mapped based on low frequency coverage. Low frequency continues downslope to the basin floor deposits indicating reservoir connectivity (Figure 50). The aggradational, accretionary margin has multiple stacked pay horizons represented by a shelf edge reef, toe-of-slope aprons and basin floor fans (Figure 51).

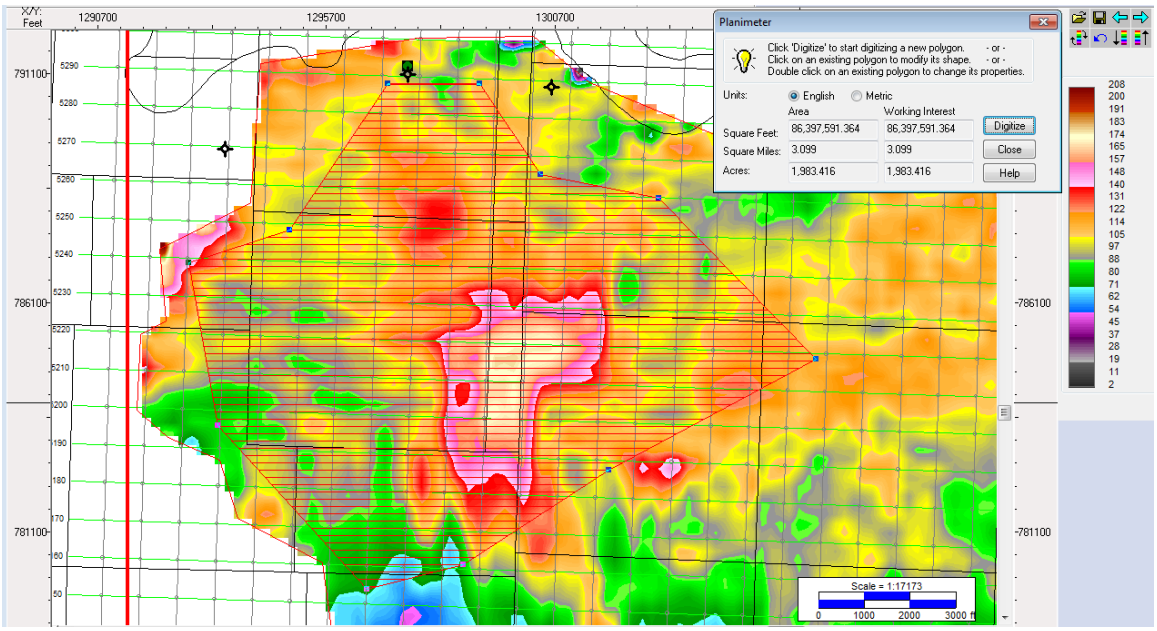

Figure 49. Northwest shelf edge reef area.

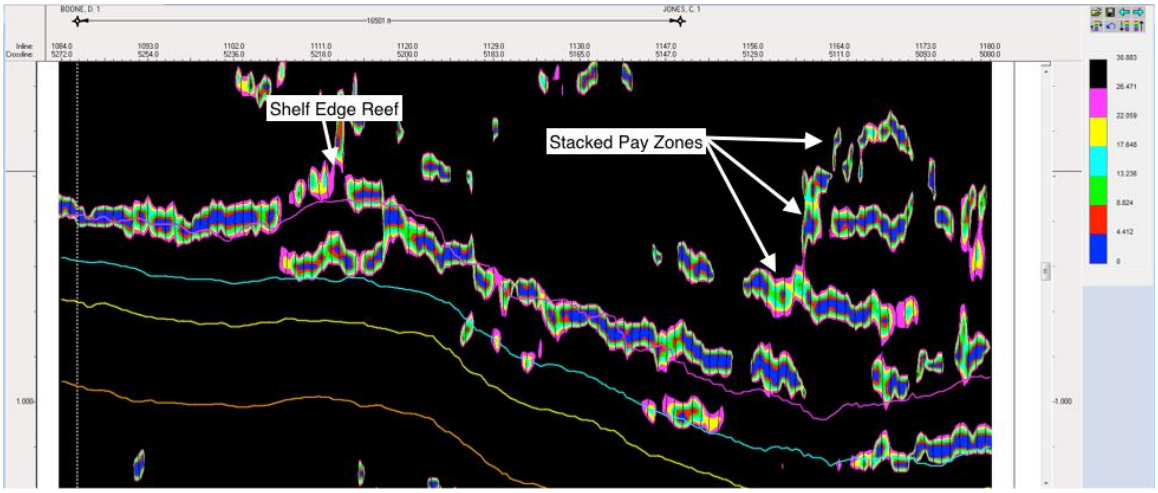

Figure 50. Northwest shelf edge reef instantaneous frequency.

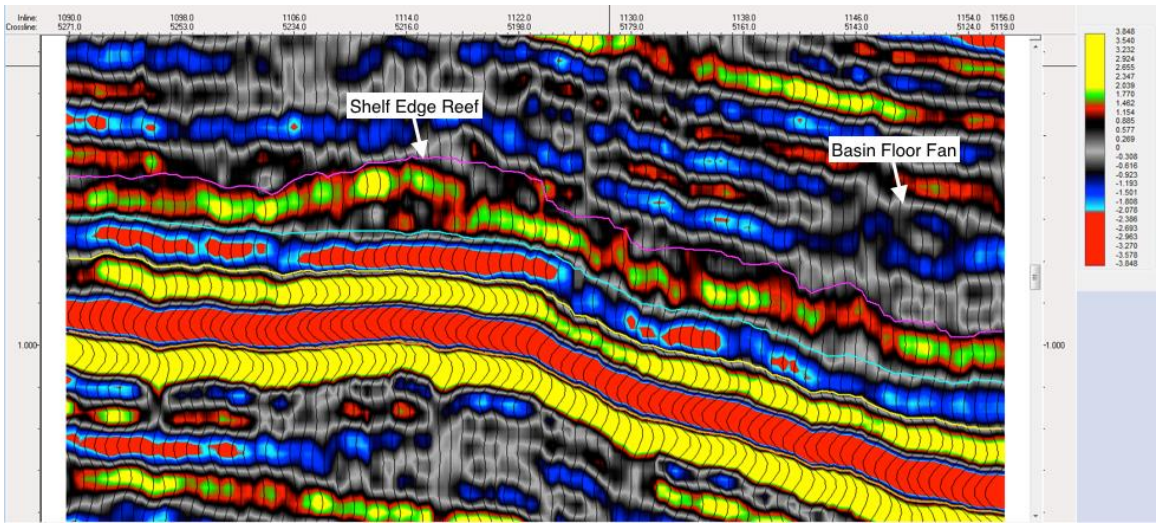

Figure 51. Northwest shelf edge reef amplitude.

Volumetric oil reserves are estimated to be 1,758,184 barrels of oil. This is purely an estimate since there is no available core or log data for the shelf edge reef. The volumetrics are based on an area of 1,983 acres, a 20-foot pay zone, 10% porosity, 10% hydrocarbon saturation, a 0.6 recovery factor and an oil volume factor of 1.05.

Chapter 7: Conclusions

Knox County saw siliciclastic marine and carbonate sedimentation from the Ordovician to the late Pennsylvanian. The Rasberry Reef carbonate mounds represent the primary reservoir lithofacies and follow Loucks and Fu's scenario two model for phylloid algal mounds. The model has a bafflestone core composed of phylloid algal bioherms with a draping *Komia*, packstone to grainstone lithofacies. Porosity development occurred during shallow and deep burial within the mound. Stylolitic seams transferred diagenetic fluid throughout the mound that contributed to the generation vuggy and moldic porosity.

Log-derived petrophysical models are reliable within a 1.5% to 3% range relative to core-derived values. Log-derived estimates of the bulk volume of hydrocarbons tended to be lower within the data set. Representative values of the tortuosity constant, *a*, cementation exponent, *m*, and saturation exponent, n, for carbonates were not reliable for all wells. Matrix composition varies throughout a reef and affects these values and their petrophysical models.

The instantaneous frequency attribute provides an effective means for finding lithology variations, widespread porosity trends, fracture zones and hydrocarbon bearing zones. The attribute was effective in finding a channel fan complex that was assumed to be a marine transgression represented by widespread black shale deposition. The channel fan complex has over five channels with each potentially being an effective hydrocarbon reservoir.

	PHIE, %			BVH, %			BVW, %			K, md		
Depth	Log	Core	Difference	Log	Core	Difference	Log	Core	Difference	Log	Core	Difference
5698.0	4.38	1.45	2.93	0.10	0.32	0.22	4.28	1.13	3.15	0.010	0.015	0.006
5699.0	5.70	1.53	4.17	1.07	0.08	0.99	4.63	1.45	3.18	0.044	0.011	0.033
5700.0	7.68	6.79	0.89	3.19	2.14	1.05	4.49	4.65	0.16	0.315	22.407	22.092
5701.0	7.86	9.89	2.03	3.48	2.15	1.33	4.38	7.74	3.36	0.384	4.725	4.342
5702.0	5.74	10.97	5.23	1.52	3.93	2.41	4.22	7.04	2.82	0.055	1.760	1.705
5703.0	3.87	11.23	7.36	0.06	4.59	4.53	3.81	6.64	2.83	0.006	4.940	4.935
Average	**5.87**	**6.98**		**1.57**	**2.20**		**4.30**	**4.77**		**0.136**	**5.643**	
5704.0	3.97	4.28	0.31	0.38	0.71	0.33	3.59	3.57	0.02	0.007	0.486	0.479
5705.0	3.51	7.77	4.26	0.00	3.51	3.51	3.51	4.26	0.75	0.003	0.501	0.498
5706.0	2.48	4.88	2.40	0.00	1.82	1.82	3.44	3.06	0.38	0.000	0.726	0.725
5707.0	1.49	3.28	1.79	0.00	1.14	1.14	3.44	2.14	1.30	0.000	0.003	0.003
5708.0	2.50	4.27	1.77	0.00	1.06	1.06	3.52	3.21	0.31	0.000	2.211	2.211
5709.0	4.03	1.59	2.44	0.00	0.38	0.38	3.67	1.21	2.46	0.008	0.092	0.085
5710.0	3.01	1.17	1.84	0.00	0.16	0.16	3.92	1.00	2.92	0.001	0.017	0.016
5711.0	2.98	4.44	1.46	0.00	1.85	1.85	4.16	2.59	1.57	0.001	4.084	4.083
5712.0	6.02	2.59	3.43	1.43	0.59	0.84	4.59	2.00	2.59	0.063	0.061	0.003
5713.0	7.43	0.86	6.57	2.50	0.20	2.30	4.93	0.66	4.27	0.212	0.004	0.208
5714.0	8.95	8.58	0.37	3.53	1.83	1.70	5.42	6.75	1.33	0.576	0.413	0.163
5715.0	10.56	10.35	0.21	4.80	2.91	1.89	5.76	7.44	1.68	1.472	4.893	3.421
Average	**4.74**	**4.50**		**1.05**	**1.35**		**4.16**	**3.16**		**0.195**	**1.124**	
5716.0	11.00	8.21	2.79	5.16	3.59	1.57	5.84	4.62	1.22	1.859	66.141	64.282
5717.0	10.61	12.01	1.40	4.62	4.48	0.14	5.99	7.53	1.54	1.403	133.460	132.057
5718.0	9.52	14.39	4.87	3.47	6.50	3.03	6.05	7.89	1.84	0.687	243.184	242.497
5719.0	9.44	13.52	4.08	3.35	6.00	2.65	6.09	7.52	1.43	0.643	562.618	561.975
5720.0	8.41	12.03	3.62	2.21	5.32	3.11	6.20	6.71	0.51	0.295	45.280	44.985
5721.0	8.01	11.13	3.12	1.56	4.15	2.59	6.45	6.98	0.53	0.200	174.018	173.818
5722.0	9.52	8.75	0.77	2.92	2.96	0.04	6.60	5.79	0.81	0.577	31.759	31.181
5723.0	10.06	9.04	1.02	3.26	3.25	0.01	6.80	5.79	1.01	0.774	13.049	12.276
5724.0	10.04	9.40	0.64	3.09	2.64	0.45	6.95	6.75	0.20	0.732	10.068	9.336
5725.0	9.05	5.60	3.45	2.02	1.26	0.76	7.03	4.34	2.69	0.368	0.540	0.172
5726.0	10.06	8.40	1.66	3.02	2.55	0.47	7.04	5.86	1.18	0.721	9.399	8.678
5727.0	10.03	4.36	5.67	3.00	0.49	2.51	7.03	3.87	3.16	0.710	0.032	0.678
5728.0	8.57	11.52	2.95	1.47	3.40	1.93	7.10	8.11	1.01	0.255	22.231	21.976
5729.0	8.02	11.12	3.10	0.92	3.64	2.72	7.10	7.48	0.38	0.167	45.958	45.791
5730.0	8.40	13.01	4.61	1.43	4.15	2.72	6.97	8.86	1.89	0.232	57.043	56.810
5731.0	7.34	10.75	3.41	0.69	3.06	2.37	6.65	7.69	1.04	0.107	13.192	13.084
5732.0	6.41	4.61	1.80	0.24	0.99	0.75	6.17	3.61	2.56	0.053	0.352	0.300
5733.0	3.99	9.41	5.42	0.00	3.91	3.91	5.57	5.50	0.07	0.003	5.332	5.329
5734.0	1.98	5.73	3.75	0.00	2.38	2.38	4.77	3.36	1.41	0.000	8.175	8.175
5735.0	0.00	6.11	6.11	0.00	3.05	3.05	0.00	3.06	3.06	0.000	1.538	1.538
Average	**8.02**	**9.45**		**2.12**	**3.39**		**6.12**	**6.07**		**0.489**	**72.168**	
5736.0	0.00	2.68	2.68	0.00	0.78	0.78	0.00	1.90	1.90	0.000	0.051	0.051
5737.0	0.00	0.70	0.70	0.00	0.18	0.18	0.00	0.53	0.53	0.000	0.004	0.004
Average	**0.00**	**1.69**		**0.00**	**0.48**		**0.00**	**1.21**		**0.000**	**0.028**	
5738.0	0.47	0.21	0.26	0.00	0.03	0.03	3.00	0.18	2.82	0.000	0.057	0.057
5739.0	0.48	0.23	0.25	0.00	0.03	0.03	3.01	0.20	2.81	0.000	0.818	0.818
5740.0	0.96	0.48	0.48	0.00	0.02	0.02	2.92	0.46	2.46	0.000	0.002	0.002
5741.0	0.99	1.08	0.09	0.00	0.23	0.23	2.90	0.85	2.05	0.000	0.003	0.003
Average	**0.73**	**0.50**		**0.00**	**0.08**		**2.96**	**0.42**		**0.000**	**0.220**	
		Average	**2.69**		Average	**1.50**		Average	**1.71**		Average	**33.656**
		STD	**1.91**		STD	**1.22**		STD	**1.10**		STD	**94.809**

References

Archie, G.E., 1942, The electrical resistivity log as an aid in determining some reservoir characteristics: Journal of Petroleum Technology, v. 5, pp. 54-62.

Asquith, G.B., 1979, Subsurface carbonate depositional models: a concise review: Tulsa, Oklahoma, PennWell Books, pp. 121.

Asquith, G., and Krygowski, D., 2004, Basic Well Log Analysis, AAPG Methods in Exploration Series, No. 16, pp. 31-142.

Bonnaffe, Florence, Eberli, Gregor P., Lomando, Anthony J., and Janson, Xavier, 1991, Seismic Characterization of Large-Scale Platform-Margin Collapse along the zhujiang carbonate platform (Miocene) of the South China Sea based on Miocene outcrop analogs from Mut Basin, Turkey *in* Cenozoic Carbonate Systems of Australasia, AAPG.

Browning, D.W. and Donovan, R.N., 1989, The Bowar Reef Complex-Stephens County, Texas in Mear, C.E. editor, Petroleum Geology of Mississippian Carbonates in North-Central Texas. Spec. Pub. Fort Worth Geological Society, pp. 93-104.

Cleaves, A.W., II and Erxleben, A.W., 1983, Upper Strawn and Canyon cratonic deposition of the Bend Arch, North-Central Texas, *in* McNulty, C.I. and

McPherson, J.G., eds., Transactions: Ft Worth, Texas, 1985 Southwest Section, AAPG, pp. 27-46.

Cleaves, A., 1993, Sequence stratigraphy, systems tracts, and mapping strategies for the subsurface Middle and Upper Pennsylvanian of the eastern shelf, *in* AAPG Southwest Section Regional Meeting: Fort Worth Geological Society, pp. 26–42.

Crain, E.R., 1978. The Rock-Fluid Model for Petrophysical Analysis *in* Crain's Petrophysical Handbook, https://www.spec2000.net/01-rockfluidmodel.htm.

Dalziel, I. W. D., Lawver, L. A., Gahagan, L. M., Campbel, D. A., and Watson, G., 2002, Texas through time Plate Model, The University of Texas at Austin, Institute for Geophysics, http://www.ig.utexas.edu/research/projects/plates/movies/Texas_Through_Time_020312.ppt.

Dewan, J., 1983, Essentials of Modern Open-Hole Log Interpretation: Tulsa, Oklahoma, PennWell Publishing Company, pp. 361.

Dunham, R.J., 1962. Classification of carbonate rocks according to depositional textures, *in* Ham, W.E., (ed.). *Classification of carbonate rocks*. AAPG Memoir 1. pp. 108-121.

Flippin, J.W., 1982, The stratigraphy, structure, and economic aspects of the Paleozoic strata in Erath County, North-Central Texas *in* Martin, C.A., ed., Petroleum Geology of the Fort Worth Basin and Bend Arch area: Dallas Geological Society, pp. 129-155.

Geary, J.R., 2008, Controls on Hydrocarbon Entrapment and Reservoir Distribution: the Pennsylvanian Big Lime and Oswego Limestone in the Putnam Field Area, Anadarko Basin, Oklahoma, Hess Corporation, HGS North American Dinner Meeting, pp. 1-45.

Grammer, M.G. and Ritter, A.L., 1996, Phylloid Algal Mounds in the Paradox Basin, southwestern U.S.A.-An alternative to the *in situ* constructional growth model, Michigan Geological Repository for Research and Education, Western Michigan Unviersity, pp. 1-38.

Gunn, R.D., 1979, Desmoinesian depositional systems in the Knox-Baylor Trough, in Hyne, N.J., ed., Pennsylvanian sandstones of the Mid-continent: Tulsa, OK, Tulsa Geological Society, pp. 221-234.

Heckel, P.H., 1986, Sea-level curve for Pennsylvanian eustatic marine transgressive-regressive depositional cycles along midcontinent outcrop belt, North America: Geology, v. 14, pp. 330-334.

Herron, D.A., 2011, First Steps in Seismic Interpretation *in* Geophysical Monograph Series, Society of Exploration Geophysicists, pp. 35-57.

Johnson, H. H., 1961, Limestone-building algae and algal limestones: Colorado School of Mines, Golden, pp. 279.

King Jr., D.T., 1990, Probable influence of early Carboniferous (Tournnaisian-early Visean) geography on the development of Waulsortian and Waulsortian-like mounds. Geology, v. 18, pp. 591-594.

Laudon, L.R., Bowsher, A.L., 1941. Mississippian formations of Sacramento Mountains, New Mexico. AAPG Bulletin v. 25, pp. 2017-2160.

Loucks, R.G. and Fu, Q.L., 2016, *Origin and Characterization of the Lithofacies and Dual Micropore/Macropore Network in Pennsylvanian (Early Desmoinesian) Caddo Shelf-Buildup Complexes, Stephens County, North-Central Texas.* GCAGS Journal, v. 5, pp. 1-24.

Morris, R.L. and Biggs, W.P., 1967, Using log-derived values of water saturation and porosity: Society of Professional Well Log Analysts, 8th Annual Logging Symposium, Transactions, Paper O.

Pollastro, R.M., Jarvie, D.M., Hill, R.J., and Adams, C.W., 2007, Geologic framework of the Mississippian Barnett Shale, Barnett-Paleozoic total petroleum system, Bend Arch-Fort Worth Basin, Texas: AAPG Bulletin, v. 91, no. 4, pp. 405-436.

Riding, R., 2001, Structure and composition of organic reefs and carbonate mud mounds: concepts and categories. Earth Science Reviews, v. 58, pp. 163-231.

Sarhan, M.A., 2017, The efficiency of seismic attributes to differentiate between massive and non-massive carbonate successions for hydrocarbon exploration activity, NRIAG Journal of Astronomy and Geophysics.

Schlumberger, 1972, Log Interpretation, Vol. I-Principles: New York, Schlumberger Limited, pp. 112.

Sloss, L.L. *Sedimentary cover, North American Craton, U.S.* Boulder, Colorado: Geological Society of America, 1988. Print.

Steiber, S.J., 1970, Pulsed neutron capture log evaluation in the Louisiana Gulf Coast: Society of Petroleum Engineers, 45th Annual Meeting, paper SPE-2961.

Timur, A., 1968, An investigation of permeability, porosity, and residual water saturation relationships for sandstone reservoirs: The Log Analyst, v. 9, p. 8-17.

Wright, W.R., 2011, Pennsylvanian paleodepositional evolution of the greater Permian Basin, Texas and New Mexico: Depositional systems and hydrocarbon reservoir analysis, AAPG Bulletin, v. 95, no. 9, p. 1525-1555.

Biographical Information

William Hoffman is from Dallas, Texas and graduated from Dallas Jesuit High School. He received his Bachelors of Science Degree in Geology with a Biology Minor from UT Arlington in 2015. He continued his education at UT Arlington by entering the Petroleum Geoscience Masters Program. He has worked as a research assistant, mine geologist and petroleum landman and intends to continue on as a petroleum geologist for an oil and gas company.